Nanoscale Advances

ROYAL SOCIETY OF CHEMISTRY

REVIEW

View Article Online
View Journal | View Issue

Cite this: *Nanoscale Adv.*, 2020, **2**, 5130

Carbon-based nanomaterials: in the quest of alternative metal-free photocatalysts for solar water splitting

Simanta Kundu, [a] Kommula Bramhaiah [b] and Santanu Bhattacharyya *[b]

One of the alarming problems of modern civilization is global warming due to the inevitable rise of CO_2 in the environment, mainly because of the excessive use of traditional fossil fuels. The gradual depletion of fossil fuels is another challenge regarding the future energy demand; therefore, alternative renewable energy research is necessary. One of the alternative approaches is the solar fuel generation by means of photocatalytic water splitting and more specifically, hydrogen evolution from water through the reductive half-reaction. Hydrogen is the cleanest fuel and does not produce any greenhouse gas upon direct combustion, or even while acting as a chemical feedstock for other transportable fuel generation. Therefore, it is desirable to produce efficient photocatalysts for solar water splitting. After the discovery of the first photocatalytic water splitting reaction by Fujisima and Honda, several advancements have been made with metal-based inorganic semiconductor photo-catalysts. However, their practical applicability is still under debate considering the environmental sustainability, stability and economical expenses. As a result, it is essential to develop alternate photocatalysts that are environmentally sustainable, cost-effective, stable and highly efficient. The metal-free approach is one of the most promising approaches in this regard. Herein, we discuss the recent developments in carbon-based materials and their hybrids as alternative metal free photocatalysts for solar water splitting. The present discussion includes g-C_3N_4, two-dimensional graphene/graphene oxides, one-dimensional carbon nanotubes/carbon nanofibers and zero-dimensional graphene QDs/carbon dots. We have focused on the rectification of exciton generation, charge separation and interfacial photochemical processes for photocatalysis, followed by possible optimization pathways of these

Received 10th July 2020
Accepted 2nd September 2020

DOI: 10.1039/d0na00569j

rsc.li/nanoscale-advances

[a]*Department of Chemistry, Shibpur Dinobundhoo Institution (College), 412/1, G. T. Road (South), Shibpur, Howrah, West Bengal, 711102, India*

[b]*Department of Chemical Sciences, IISER Berhampur, Transit Campus (Govt. ITI), Eng. School Road, Berhampur, Odisha, 760010, India. E-mail: santanub@iiserbpr.ac.in*

Dr Simanta Kundu obtained his B.Sc and M.Sc in Chemistry from the University of Calcutta. He received his Ph.D. from Jadavpur University, Kolkata, India in 2015, then he worked as a Research Associate in the Department of Materials Sciences, IACS, Kolkata, and as a Visiting Fellow in the Department of Chemical Sciences, Tata Institute of Fundamental Research, Mumbai, India. He is currently an Assistant Professor in the Department of Chemistry of Shibpur Dinobundhoo Institution (College), Howrah, India since July 2017. His research interest includes the synthesis and characterization of different colloidal semiconducting QDs and hybrid materials for light-harvesting applications.

Dr Kommula Bramhaiah received his M.Sc from the Department of Chemistry in 2011 at Jawaharlal Nehru Technological University Anantapur, Andhra Pradesh, India. He then joined Dr Neena S John's group as a Ph.D. student. He received his Ph.D. in 2018 from the Centre for Nano and Soft Matter Sciences, Bangalore, India. Currently he has moved to the Indian Institute of Science Education and Research (IISER), Berhampur, India for his post-doctoral research under the supervision of Dr Santanu Bhattacharyya. His research interests are mainly on strategic materials design for energy applications include water splitting, energy storage and catalysis.

typical all carbon-based materials. Finally, we have highlighted several fundamental challenges and their possible solutions, as well as the future direction on this particular aspect.

1. Introduction

The supply of sustainable energy is a major key to the development of modern civilization. At present, more than 80% of the global energy supply is mostly dependent on the burning of fossil fuels.[1] However, the fossil-fuel reserves are limited, and at current rates of consumption, they will be depleted in the near future.[2] Beyond this, the use of fossil-fuels generates toxic emissions that are a great threat to the environment. Among the emitted gases, CO_2 released in the burning of all fossil-fuels raises concerns about its impact on the global climate and highlights the need to reduce emissions.

In order to reduce the emission of CO_2, it is necessary to develop green-technologies as alternate energy supplies to fossil-fuels. This has led to the development of technologies to utilize the most naturally abundant energy from the sun because the amount of energy reaching us every hour is nearly twice that of the world's annual energy requirements.[3] Thus, important developments have been achieved in harnessing solar energy to produce electricity using solar cells. However, due to the diurnal variation in sunlight and weather variability, the electricity produced by solar cells needs to be stored for later use during periods of darkness. This storage requires significant investment in infrastructure, which makes it difficult to utilize solar energy as an alternative green energy re-source.

As an alternative, the production of chemical fuels by harvesting solar energy has been seen as a solution to these problems. In this method, solar energy is stored by the formation of high-energy compounds from water and carbon dioxide and the stored energy can be then released at the time of need by combustion.[4] Chemical fuels are attractive media for energy storage because of their very high specific energies. The two prominent methods for producing chemical fuel are (a) water splitting – *i.e.* converting water to produce hydrogen fuel; (b) CO_2 utilization – converting CO_2 into fuel (*e.g.* methane or methanol) or useful chemicals (*e.g.* carbon monoxide or formic acid).[5–9] Among these two, water splitting has received significant attention because the reactants water and sunlight are abundant and practically inexhaustible. Moreover, the specific energy of hydrogen is extremely high (142 MJ kg^{-1}), almost three times higher than gasoline and even a few orders of magnitude higher than lithium-ion batteries.[10] In addition, the combustion of hydrogen fuel is completely clean and it never produces any greenhouse gases. Furthermore, one can store it and can be utilized whenever required.[11]

There are two major techniques, namely, photoelectrochemical and, photocatalytic water splitting, which generate hydrogen *via* water-splitting using solar energy.[12] In photoelectrochemical water splitting, a photocurrent is generated and then with that generated bias, the water splitting reaction is carried out in the presence of electrocatalysts. On the other hand, photocatalysis occurs in an integrated single system where light absorption and chemical reactions occur without any external circuitry or bias. Photocatalytic hydrogen production employs semiconductor photocatalysts that absorb solar photons and are dispersed in aqueous medium or grown/deposited on a support, and create electron–hole pairs for water redox reactions upon irradiation.[13,14] For the photocatalytic water splitting reaction, the mandatory conditions are as follows. (a) The highest valence band level of the photocatalyst should be more positive with respect to the water oxidation potential (+1.23 V *vs.* NHE). (b) The lowest conduction band (CB) level has to be more negative with respect to the reduction potential of H^+ (0 V *vs.* NHE).[15] However, the back reaction for the reformation of H_2O from H_2 and O_2 is also feasible. To overcome this back reaction, the separation of the two reaction sites is important. One can use co-catalysts (both metal and non-metal-based) that can increase the active sites for photocatalytic reactions and also trap the free carriers, which will be further utilized for photocatalysis. Another approach is to use electron and/or hole scavengers that can consume one type of carrier and facilitate the reaction on the other end. Therefore, the development and fine-tuning of the photocatalyst material are the key challenges as both half-reactions proceed in the same reaction vessel, and the prevention of various back reactions and product extraction are critical for achieving high efficiency. After the discovery of the first photocatalytic water splitting reaction by Fujishima and Honda in 1972,[16] TiO_2 has become the highest investigated semiconductor for photocatalytic water splitting. This is because it is easily available, cheap, nontoxic and chemically inert. Negative reduction potential (compared to the proton reduction process) and positive oxidation potential (compared to the water oxidation process) promote the complete water splitting process on the surface of TiO_2. However, the bandgap of TiO_2 is extremely wide (~3.5 eV), resulting in the lack of visible light absorption

Dr Santanu Bhattacharyya received his Ph.D. (Science) from the Indian Association for the Cultivation of Science, Kolkata in 2013. He was subsequently a postdoctoral scientist in IMDEA Nanociencia, Madrid, and later in 2015, he joined the Chair for Photonics and Optoelectronics, LMU, Munich, as an Alexander Von Humboldt fellow. After finishing his postdoctoral stay in Germany, he has joined as an Assistant Professor in the Department of Chemical Sciences, IISER Berhampur since August 2018. His group mainly focuses on several light-induced processes in fluorescent nanomaterials and the optimization of environmentally sustainable nanomaterials for solar fuel generation.

throughout the whole solar spectrum range. However, several approaches have already been made to overcome this; *e.g.*, photosensitization by dyes/semiconductors, elemental doping, attachment of plasmonic metal nanoparticles, *etc.*[17–20] Visible-light-absorbing inorganic semiconductors made of transition metal chalcogenide, oxide and nitride nanocrystals have already been discussed extensively as efficient photocatalysts for solar light-driven photocatalytic water splitting,[18,21–26] although the practical applicability and commercialization remain questionable due to very low catalytic efficiencies. The main reasons behind this low catalytic efficiency are free carrier recombination at the grain boundaries and bulk defects within photocatalysts with considerable diffusion paths for charge carriers and fewer redox-active sites.[27,28] High toxicity, hard synthetic procedures, poor sustainability and mostly higher economical expenses further limit their applications.[29–31] Therefore, we need a cheap, robust and environmentally sustainable material having a greater visible-light-absorption cross-section and efficient internal charge transfer process.[32–35] In contrast to the traditional metal-based photocatalytic systems, a new generation of alternative metal-free photocatalysts has already begun with the evolution of carbon-based polymeric carbon nitride in recent years. Carbon nitrides are completely metal-free materials made of earth-abundant carbon and nitrogen. Carbon nitride can be easily fabricated from easily available nitrogen-rich precursors (*e.g.*, melamine, urea, thiourea, chitosan, *etc.*). Moreover, modified optoelectronic features, large specific surface area, physicochemical stability and efficient charge transport features make it an efficient new-generation photocatalyst for solar light-driven hydrogen evolution reactions. Beyond this, recent reports have highlighted the promising photocatalytic features of other carbon-based materials and their hybrids (*e.g.*, carbon dots, graphene QDs, graphene oxides, *etc.*). Although the progress is still very limited, there are plenty of opportunities to overcome the practical challenges, especially regarding the metal catalyst-free approach.

Considering the current demand, we have mainly focused on the very recent progress of carbon-based materials as an alternative class of efficient photocatalysts (Fig. 1). Very precisely, we have highlighted metal-free approaches, keeping in mind the progress of more environmentally sustainable, more robust, efficient and economically cheaper ideas for photocatalytic solar fuel generation. In addition to the carbon nitride systems, we have discussed the several promises of new metal-free photocatalysts made of carbon dots, graphene QDs, graphene oxide-based hybrids and intrinsic heterojunction dyad-like structures. We have confined our discussion to different carbon-based new materials and the fundamental understanding behind the overall photophysical and photochemical processes, followed by several strategies to optimize the new materials for future applications as efficient photocatalysts.

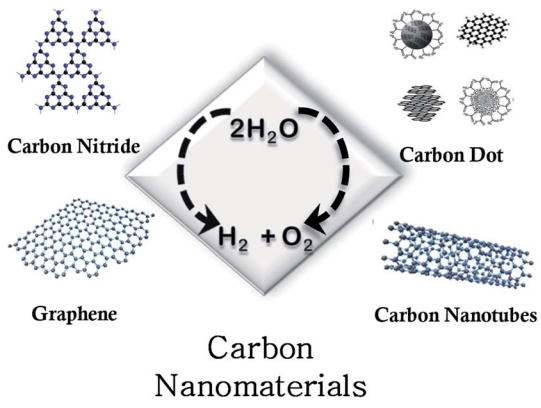

Fig. 1 Schematic representation of different carbon-based nanomaterials.

2. Thermodynamics related to photocatalytic solar water splitting

Photocatalytic water splitting is an energetically uphill reaction where water molecules split into H_2 and O_2 by means of both the reductive half-reaction of the proton to hydrogen and the oxidative half-reaction of water to oxygen. The free energy change for the overall water splitting is 237 kJ mol^{-1}.[8,13] Therefore, as per the Nernst equation, the required minimum energy for overall water splitting is 1.23 eV. Theoretically, all semiconductors having a bandgap of 1.23 eV or more will be suitable for photocatalytic water splitting. In practice, it is completely ambiguous. We have to consider the required overpotential and reorganization energy for the interfacial charge transfer process,[36] therefore, semiconducting photocatalysts having a bandgap of 1.23 eV are not practically suitable for photocatalytic water splitting.[37,38] It is already well established that the minimum bandgap required for photocatalytic water splitting is ~2 eV.[39] Beyond this, overall photocatalytic reactions include the following consecutive steps.[15] (a) Solar light harvesting by efficient antenna materials; (b) exciton generation and charge separation; (c) free carrier transport towards the interface; (d) photochemical redox reactions. As mentioned before, as per the thermodynamics, wider bandgap semiconductors are efficient for photocatalytic water splitting. On the other hand, it can also decrease the extent of the solar light-harvesting process. Therefore, one has to balance these two aspects to satisfy thermodynamic constraints along with efficient visible light absorption. Under a broad range of illumination, photocatalysts eventually absorb light with different energies. If the photon energy is greater than the bandgap of the catalyst, it leads to the formation of photoinduced excitons, which are excited electrons in the conduction band, and counter holes in the valence band. After the generation of the excitons, the electrons residing in the conduction band can recombine with the remaining holes through both radiative and non-radiative recombination processes. Radiative and non-radiative recombinations are typical competitive processes that can decrease the free carriers. The free carriers can survive the overall recombination processes and can only reach the interface through diffusion or an electric field, followed by reductive and oxidative half-reactions. Considering the time-scale, light-induced exciton generation is a transient process (femtosecond time-scale), while both radiative and non-

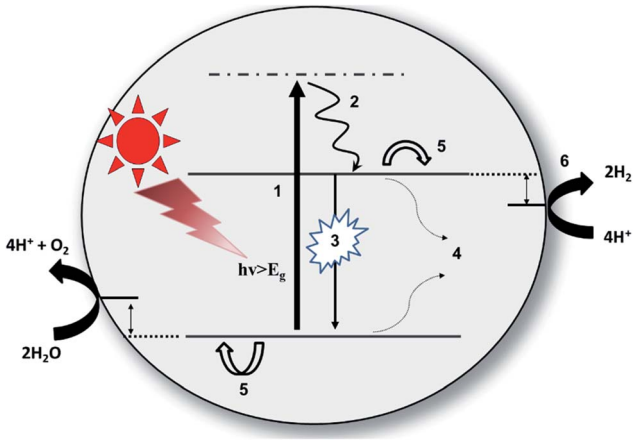

Fig. 2 Schematic representation of different photophysical processes on a semiconducting photocatalyst upon light irradiation: (1) light absorption, (2) thermal relaxation, (3) radiative recombination, (4) nonradiative recombination, (5) diffusion of the free carriers, (6) photochemical redox reactions.

radiative recombination processes happen in the picosecond to nanosecond time-scale (however, recombination through the triplet state, in general, can reach time-scales of a few hundred nanoseconds to milliseconds). Diffusion and charge separation of the free carriers also happen on a similar time-scale. However, photochemical redox reactions (both oxidative and reductive) on the surface are comparatively slower processes (~microsecond scale).[40] It is always crucial to regulate the overall photophysical and consecutive photochemical processes to enhance the efficiency of the overall photocatalytic solar water splitting (Fig. 2). Carbon-based semiconducting photocatalysts (*e.g.*, carbon nitrides, reduced graphene oxides, graphene QDs, carbon dots, *etc.*, as well as their metal-free hybrids) are among the emerging classes of materials that have suitable bandgaps (≥2 eV) for efficient solar light absorption and they also possess sufficient overpotentials and reorganization energies to satisfy the required thermodynamic criteria. Several structural (physical and/or chemical) and elemental defects can facilitate free carrier accumulation on the surface without using any additional metal catalyst.

3. Carbon nitride-based photocatalysts

Among all the allotropes of C_3N_4, graphitic C_3N_4 (g-C_3N_4) shows maximum stability in ambient medium and larger applicability for solar light-driven photo-catalysis.[41] Keeping in mind the kinetic and thermodynamic features of g-C_3N_4, there are commonly three possible approaches to optimize this material for efficient photocatalysis. (a) Enhancing the visible light absorption by optimizing the bandgap, (b) increasing the number of free carriers by reducing competitive radiative and non-radiative recombination processes, and (c) enhancing the active sites on the surface accessible for photochemical redox reactions.

The graphitic plane of g-C_3N_4 consists of tris-*s*-triazine/melem units connected by the planar amino groups (Fig. 3a). The controlled condensation technique by precise thermal treatment during synthesis critically regulates the in-plane molecular organization of tris-*s*-triazine units and compression of the successive planes. Therefore, one can easily tune the overall optoelectronic properties by simply varying the extent of the condensation reaction.[42] In general, the calculated bandgap of g-C_3N_4 lies around 2.5–2.7 eV, which is sufficient for overcoming the potential barrier for endothermic water splitting reaction (predicted ~1.3 eV); the absorption spectra of pristine g-C_3N_4 further support this (Fig. 3b). In addition, density functional theory calculations have predicted that the calculated bandgap of the basic melem unit is considerably higher as compared to its polymeric form. Moreover, the non-isotopic band structure is dispersed along the direction of the polymer chain (Fig. 3c).[42,43] Considering all the above-mentioned factors, the visible light absorption cross-section of g-C_3N_4 can be simply increased by increasing the degree of polymerization. Calculated data showed that the nitrogen P_Z orbital contributes to the valence band of g-C_3N_4, whereas the conduction band is directly affected by the combinations of the carbon P_Z orbitals of the g-C_3N_4 plane. Therefore, after sufficient light absorption, the photoinduced holes can reside on the nitrogen atoms and the counter electrons would be situated on the carbon atoms, which would eventually increase the charge separation process in the 2-D plane. Therefore, overall photocatalytic water splitting to hydrogen and oxygen is quite feasible, even for pristine g-C_3N_4 (Fig. 3d).[42] Simultaneous protonation with increasing the amount of polymerization can also play a crucial role in the enhancement of the photocatalytic efficiency for solar hydrogen generation (*ca.* 20 000 μmol h^{-1} g^{-1} under full arc) with higher turnover number due to the preferential modification of the conduction band accessible for the reductive half-reaction of protons.[44]

The co-polymerization of the melon unit with the organic monomer or, more specifically, molecular doping, is another alternative approach to decrease the bandgap and tune the optoelectronic properties in general. For example, the copolymerization of 2,4,6-triaminopyrimidine with melamine increases the absorption shoulder in the visible region.[45,46] Likewise, the incorporation of electron-rich molecules inside the 2-D carbon nitride domain can promote the re-localization of π-electrons, resulting in the modification of the band gap.[35,47] For example, the incorporation of 3-aminothiophene-2-carbonitrile (ATCN) in g-C_3N_4 can alter both the surface and bulk features, resulting in the up-lifting of the HOMO by 0.36 eV and the down-shifting of the LUMO by 0.18 eV. As a result, the overall bandwidth decreases to 0.54 eV (depicted in Fig. 4a).[48] The non-planar nature of the occupied and unoccupied frontier molecular orbitals promotes electron–hole separation (Fig. 4b), followed by an increase in H_2 generation, as compared to pristine g-C_3N_4 (Fig. 4c), by one order of magnitude. Efficient visible light absorption also contributes to the photocatalytic hydrogen generation after the incorporation of ATCN (Fig. 4d).[48] However, in contrast to the previous approach, Zou and coworkers have demonstrated the critical role of the electron-deficient

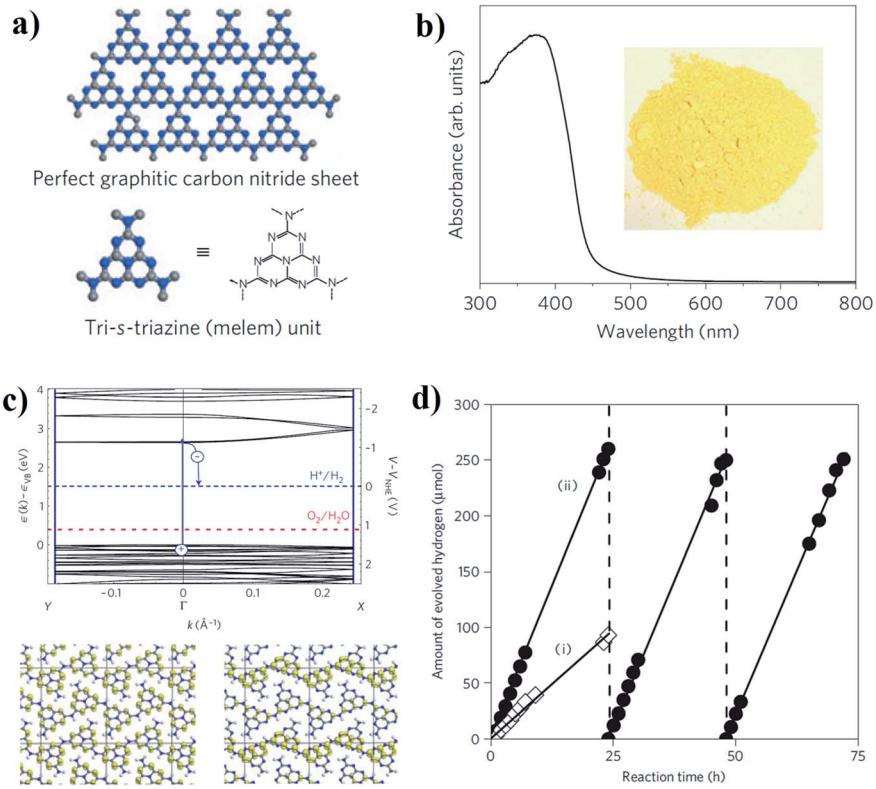

Fig. 3 (a) Structure of a perfect graphitic carbon nitride nanosheet made of basic melem units. (b) Ultraviolet-visible diffuse reflectance spectrum of the polymeric carbon nitride, and a photograph of the photocatalyst. (c) DFT-based band structure of polymeric melon, along with the reduction potential of H^+ to H_2 and the oxidation potential of H_2O to O_2 (upper panel), Kohn sham orbitals of the valence band (lower panel left) and conduction band (lower panel right). (d) Stable hydrogen evolution from carbon nitride with 24 h of repeated evacuation [(i) pure carbon nitride, (ii) 3 wt% Pt deposited]. Reprinted with permission from ref. 42. Copyright 2009 Nature Publishing Group.

pyromellitic dianhydride (PMDA) into the 2D-network of g-C_3N_4.[49] As a result, the effective valence band position decreases, resulting in the enhancement of the photooxidation reaction. Therefore, the active g-C_3N_4 modified with PMDA showed an efficient water oxidation reaction with respect to the water reduction reaction. On the other hand, as an alternative approach to molecular modification, Liu *et al.* developed a composite catalyst made of g-C_3N_4 and surface coupled CBV^{2+} as an electron mediator through hydrogen bonds.[50] This surface-attached redox mediator can enrich active sites for co-catalyst attachment and increase the photoinduced electron transfer process towards the interface; as a result, the photocatalytic hydrogen generation dramatically increases.

Alternatively, defect domains and specified disorders in g-C_3N_4 can also help to enhance the overall charge transfer process, which eventually enhances the photocatalytic water splitting efficiency.[51,52] More specifically, defects related to the nitrogen vacancies in the aromatic domain of g-C_3N_4 can increase the photocatalytic efficiency. Nitrogen vacancies can modify the active sites on the surface for free carrier accumulation and also tune the bandgap, as well as the overall optoelectronic properties of g-C_3N_4.[53] As an example, Yu *et al.* explained the bandgap tunability of the carbon nitride system by introducing nitrogen vacancies into the g-C_3N_4 framework (Fig. 5A and B) through a facile KOH-assisted method from urea as a molecular precursor. Detailed DFT calculations and partial density of states calculations show that nitrogen vacancies create a defect state about 1.52 eV above the valence band (Fig. 5C and D), which enhances the visible light absorption. Furthermore, the nitrogen-vacancy-related defect states can also enhance the charge separation, which further facilitates the photocatalysis process (Fig. 5E and F). In addition, –CN functionality on the edge of g-C_3N_4 further lowered the conduction band, which enhanced the visible light absorption.[54] Besides, distortions in the graphitic domain by increasing stacking defects, grain boundaries and termination sites on the edge of the ring can also increase the catalytic efficiency.[55] Likewise, chemical defects on the peripheral sites can further facilitate the catalytic process.[56–58] Recently, Lotsch and coworkers reported the effect of excess urea on the peripheral sites of carbon nitride, which helped to increase the charge transfer process towards the outer surface.[59]

Morphological variations in nanostructured g-C_3N_4 material can directly regulate the chemical, physical and optical properties. Most importantly, 1-D nanorods/nanotubes, 2-D sheet-like and 3-D porous structures have been well investigated to date.[47] A few recent reports have demonstrated the enhancement of solar light harvesting and charge separation kinetics for a specified shape-controlled microstructure of g-C_3N_4, which is quite like normal QDs.[40,60,61] It is noteworthy that hierarchical

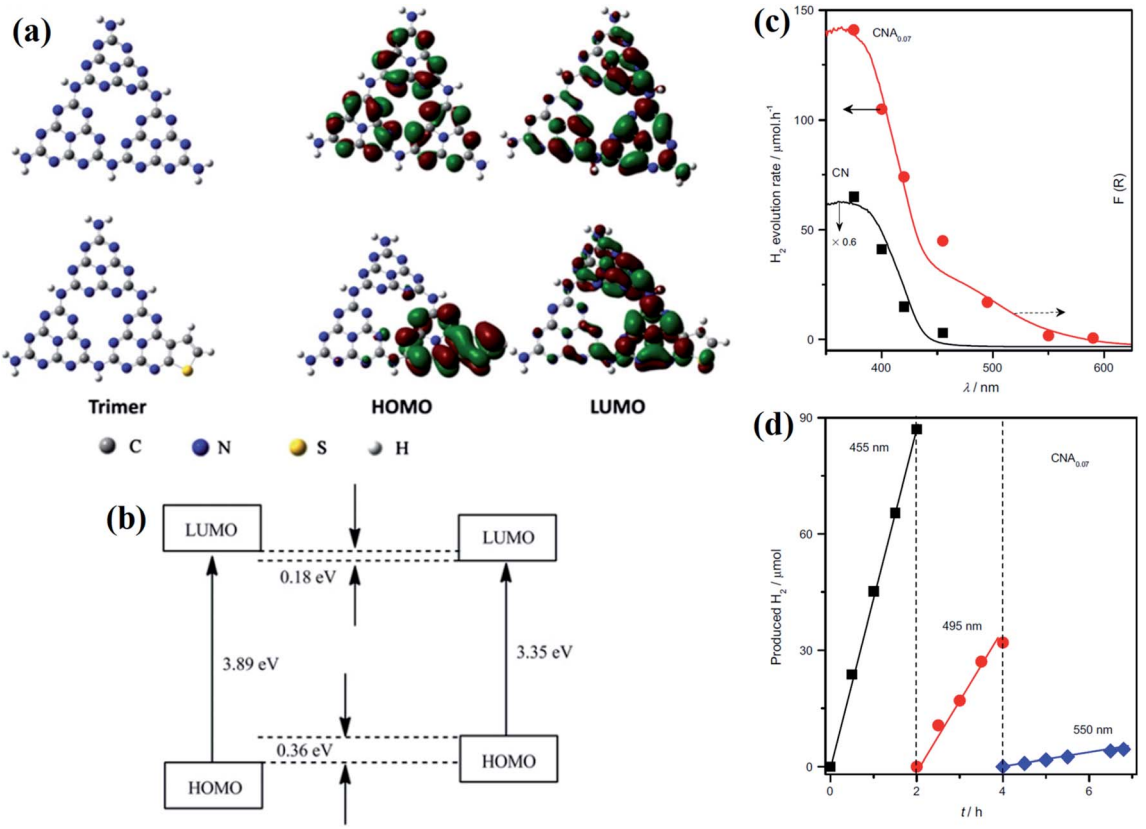

Fig. 4 (a) Electronic structure and the corresponding HOMO and LUMO for the CN trimer (upper panel) and the CNA trimer (lower panel). (b) DFT-calculated HOMO–LUMO gap. (c) Wavelength-dependent hydrogen evolution. (d) Time-dependent hydrogen evolution at different wavelengths. Reprinted with permission from ref. 48. Copyright 2013, Elsevier Inc.

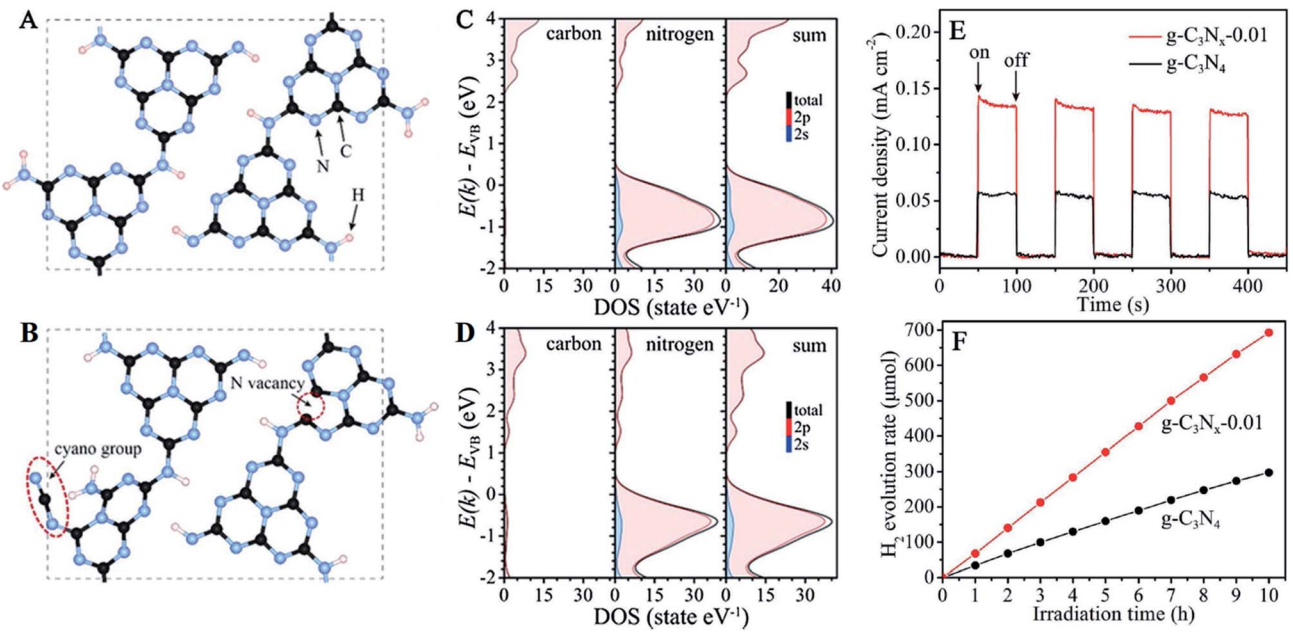

Fig. 5 The structure models of g-C_3N_4 (A) and g-C_3N_x, along with the CN group and N vacancy (B). The calculated partial densities of states for g-C_3N_4 (C) and g-C_3N_x (D). The transient photocurrent responses (E) and time courses of hydrogen evolution (F) of g-C_3N_4 and g-$C_3N_{x-0.01}$ under visible-light illumination ($\lambda > 420$ nm). Reprinted with permission from ref. 54. Copyright 2017, WILEY-VCH Verlag GmbH & Co. KGaA, Weinheim.

porous microstructures show higher photocatalytic efficiencies as compared to the bulk analogues due to higher effective surface areas and unidirectional photo-induced charge migration processes towards the surface without specific recombination.[62,63]

Beyond the structural and morphological optimizations, one of the most important metal-free alternative approaches to photocatalysis is to incorporate non-metals (*e.g.*, B, S, O, P, I, *etc.*) inside the carbon nitride matrix.[35,64,65] The incorporation of nonmetal ions generally increases the solar light absorption by narrowing the bandgap. However, it also facilitates the mobility of free carriers and enhances the active sites in the g-C_3N_4 matrix. Among all other nonmetals, 'P' is well known to enhance the visible light absorption cross-section to some extent by lowering the effective band gap.[66,67] P-doping can also significantly improve the conductivity of the pristine materials by a few orders of magnitude. Most importantly, P-doped g-C_3N_4 has a higher mid-bandgap energy (−0.16 eV *vs.* SHE) that thermodynamically favors the electron transfer process for protons and produces H_2 under visible light.[68] Considering the atomic size and electronic configuration, the 'P' atom can replace the 'C' atom and 'N' atom, and can also be incorporated interstitially. Moreover, different hierarchical structures made of P-doped carbon nitrides (*e.g.* nanoflowers, nanotubes, 2-D nanosheets, nanorods, *etc.*) can increase the photocatalytic efficiency by reducing the effective charge transfer rate towards the interface for efficient photochemical reactions/redox reactions for photocatalysis.[66–70]

The fabrication of metal-free all organic hybrids based on g-C_3N_4 is another alternative approach in this regard. As an example, π-conjugated organic materials (semiconducting polymers/oligomers) have been utilized to make intimate hybrid heterostructures with g-C_3N_4 for photocatalytic water splitting.[35] On combining with the 2D domain of g-C_3N_4, π-conjugated organic materials can act as both charge-transporting and charge-storing domains, which inhibits the competitive charge carrier recombination on the g-C_3N_4 matrix.[71,72] In a recent report, Peng and his group observed efficient photocatalytic H_2 generation (3045 μmol h^{-1} in the presence of ascorbic acid as hole scavenger) in the P3HT/g-C_3N_4 heterojunction under the illumination of visible light (Fig. 6a).[73] Normally, P3HT shows a large absorption cross-section throughout almost the entire solar spectrum, resulting in an efficient photosensitizer, while combining with a semiconducting catalyst with proper bandgap alignment (Fig. 6b). Considering the efficient hole-transporting properties of P3HT, the counter electrons can be easily injected into the g-C_3N_4 matrix through this interfacial heterojunction. As a result, the photocatalytic activity of this hybrid system increases under visible light (≥500 nm) (Fig. 6c). Alternatively, the interfacial attachment of multiwalled carbon nanotubes on g-C_3N_4 can also enhance the photocatalytic efficiency up-to 2.5-fold as compared to pristine g-C_3N_4.[74] Carbon nanotubes also possess long-range effective π-conjugation, which further increases the electron–hole separation upon light irradiation, followed by efficient free carrier transport. However, the necessity of noble

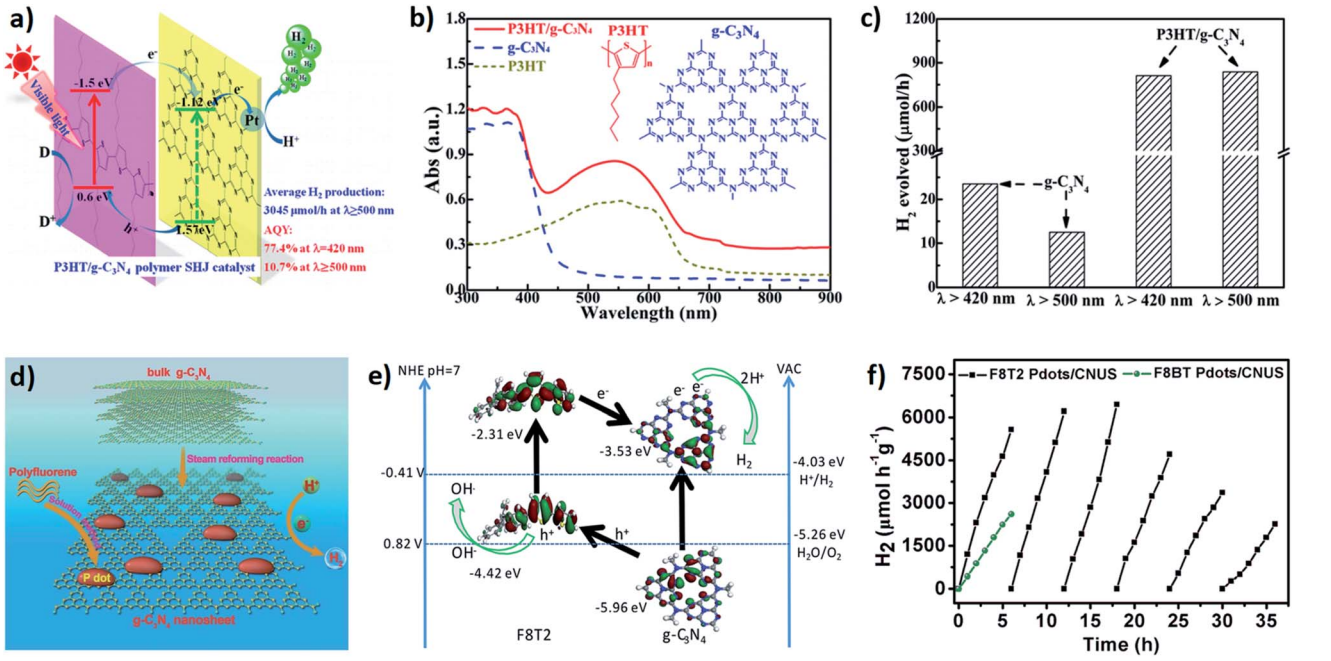

Fig. 6 (a) Schematic representation of the P3HT and g-C_3N_4 composite with efficient hydrogen generation. (b) DRS spectra of g-C_3N_4, P3HT and the composite catalyst (3 wt% P3HT/g-C_3N_4). (c) Wavelength-dependent hydrogen evolution for pure g-C_3N_4 and the composite system, respectively. Reprinted with permission from ref. 73. Copyright 2015, American Chemical Society. (d) Schematic representation of the polyfluorene nanoparticles and carbon nitride composite. (e) HOMO and LUMO alignments and charge separation mechanism of polyfluorene nanoparticles and the g-C_3N_4 composite. (f) Time-dependent hydrogen evolution for the polymer dots and g-C_3N_4 composite system. Reprinted with permission from ref. 75. Copyright 2019, the Royal Society of Chemistry.

metal co-catalysts limited the practical applicability while considering the cost-effectiveness of this typical hybrid material.

As a step forward, very recently Zhou *et al.* fabricated an aqueous dispersible all-organic composite system by combining polyfluorene-based conjugated polymer dots (Pdots) with a two-dimensional graphitic C_3N_4 system.[75] Self-assembled polyfluorene dots possess a longer excited-state lifetime with an appropriate bandgap, which enhances the visible light absorption. Therefore, the typical composite system of polyfluorene dots combined with the few-layered porous g-C_3N_4 system can harvest solar light, followed by efficient charge separation in the interface (Fig. 6d and e). Consequently, the photocatalytic hydrogen production efficiency increases with the apparent quantum yield of ~5% under visible light (Fig. 6f).

In this context, Liu *et al.* developed another promising all-organic hybrid system by combining g-C_3N_4 with carbon dots for overall water splitting *via* a stepwise two-electron/two-electron mechanism.[76] In the initial two-electron process, water was mainly oxidized to H_2O_2 and H_2 and after that, H_2O_2 decomposed into O_2 and H_2O; this step-wise process, therefore, made the overall water splitting quite faster. They have shown that in the composite system, the reduction level for H_2 was lower in energy than the conduction band, while the oxidation potential for H_2O to H_2O_2/O_2 was just above the valence band, which enhanced the possibility for the overall water splitting to both H_2 and O_2. In the composite, the C_3N_4 counterpart promoted the first step of the electron transfer process after photosensitization, *i.e.* the conversion of H_2O to H_2 and H_2O_2; on other hand, embedded carbon dots inside the C_3N_4 matrix facilitated the decomposition of H_2O_2 to O_2 and H_2O. On increasing the loading amount of carbon dots in the C_3N_4 matrix, the catalytic efficiency in visible light increased due to the increasing sub-band levels in the actual band gap of C_3N_4, which induced the photoactivity towards the longer wavelength region (>500 nm). Wei *et al.* recently developed another hybrid heterostructure by combining the aromatic carbon ring (C_{ring}) with C_3N_4 in the 2D plane by stepwise thermal treatments (namely condensation and polymerization).[77] Nitrogen lone pairs of heptazine units facilitated the formation of an in-plane heterojunction upon interfacial binding with the carbon ring (Fig. 7a). This typical in-plane π-conjugated hetero structure enhances the delocalization of the free carriers depending on the intrinsic driving force based on the different work functions of the two counterparts. Furthermore, the narrowed bandgap (Fig. 7b) enhanced the visible light absorption followed by free carrier generation and their transport towards the interfacial redox-active sites. Notably, the free carrier diffusion length and lifetime increased to a larger extent. As a result, the C_{ring}–C_3N_4 heterostructure successfully splits pure water into H_2 and O_2 without using any sacrificial reagents under light irradiation at a much higher rate as compared to pristine g-C_3N_4 (Fig. 7c).

Elemental phosphorous (especially red and black phosphorous) has become another emerging class of nonmetallic materials that can act as efficient photocatalysts. However, the fabrication of heterojunction hybrid systems upon combining black/red phosphorous with carbon-based nanomaterials can further increase the solar hydrogen generation efficiency. In a recent report, Majima *et al.* developed a two-dimensional intrinsic heterojunction by combining 2-D black phosphorous and g-C_3N_4.[78] This typical composite system showed hydrogen generation efficiency under light sources >420 nm and >780 nm.

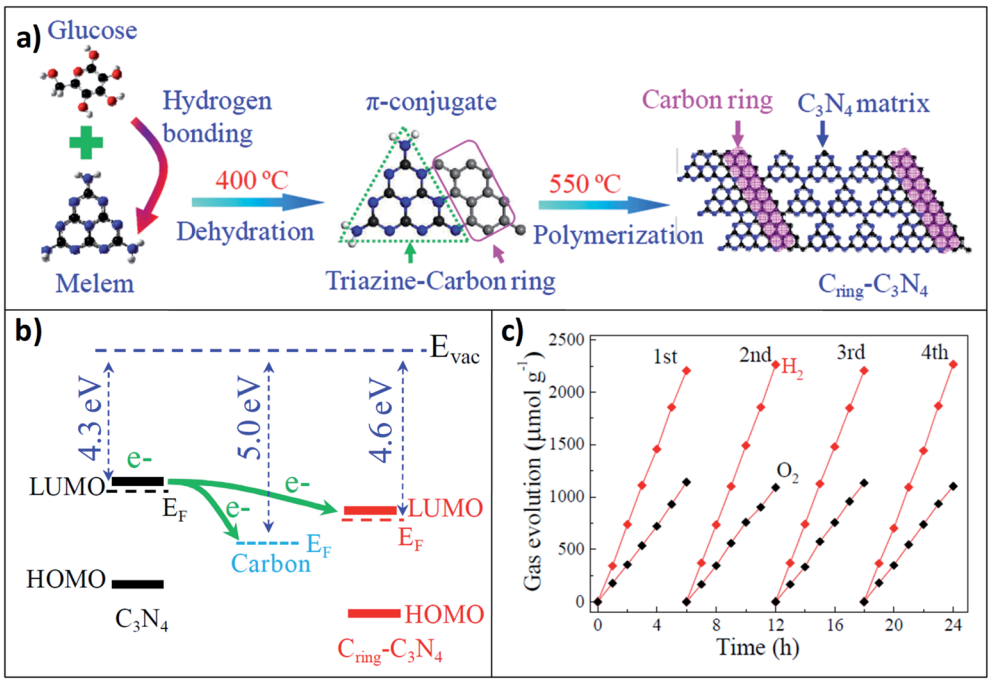

Fig. 7 (a) Schematic representation of the synthetic route of the in-plane heterostructured g-C_3N_4 and carbon ring. (b) Fermi energy level diagram for pristine g-C_3N_4, carbon, and C_{ring}–C_3N_4; (c) the H_2 and O_2 evolution rates under repeated evacuation for the C_{ring}–C_3N_4 heterojunction. Reprinted with permission from ref. 77. Copyright 2017, American Chemical Society.

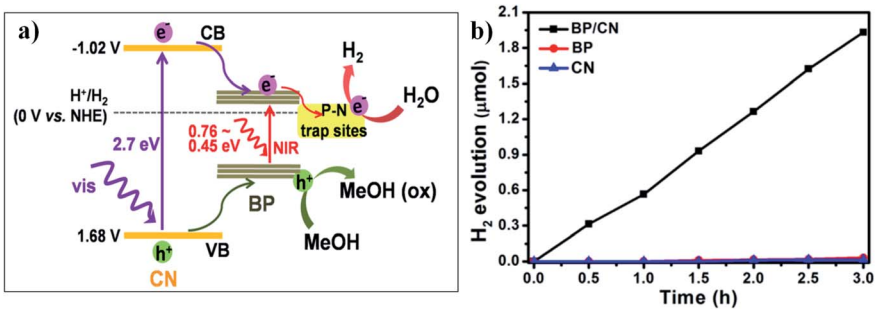

Fig. 8 (a) Schematic representation of the bandgap alignments and photocatalytic H_2 evolution for the carbon nitride and black phosphorous composite system in the presence of methanol as a hole scavenger. (b) Photocatalytic hydrogen evolution rate for different photocatalysts under visible light irradiation (in the presence of 20% methanol). Reprinted with permission from ref. 78. Copyright 2017, American Chemical Society.

Considering the bandgap alignment of both layered black P and g-C_3N_4, a type-I heterojunction can be imagined at their interface. With visible light excitation of g-C_3N_4, the photoexcited electrons are transported from g-C_3N_4 to two-dimensional black P (Fig. 8a). Due to the intimate interactions at the interface between these two counterparts, the P–N bonds create deep trapped states, which accumulate the photoinduced electrons. These free electrons can be further utilized efficiently for photocatalytic hydrogen generation in the presence of methanol as a scavenger. However, under illumination at >780 nm, 2D black phosphorous gets directly excited and the photoexcited electrons get further trapped in the deep trapped state due to the interfacial P–N bond, followed by the same photocatalytic proton reduction process as mentioned before. Pure black phosphorous is not an active catalyst because of the fast recombination process between electrons and holes, which decreases the free carriers for photocatalysis (Fig. 8b). Therefore, P–N trap sites in the composite system are necessary for efficient photocatalysis.

4. Two-dimensional graphene-based photo-catalysts

Among all the carbon-based materials, semiconducting graphene and their derivatives are one of the most promising materials for efficient photo-catalysis due to their intriguing electronic features and efficient defect mediated redox active sites.[79] Graphene is a tightly packed honeycomb-like monolayer structure with sp^2 hybridized C–C bonds (Fig. 9a) and extended delocalized π-electron clouds, resulting in a zero-bandgap semimetal with the valence band and conduction band touching at the Brillouin zone corners.[80,81] Consequently, along this two-dimensional planar structure, the free carriers' diffusion path length decreases, and the electron mobility and broad-range solar light-harvesting capability increase.[27] In general, the optoelectronic, mechanical and thermal conductive properties of graphene are almost similar to well-known single-walled carbon nanotubes.[82] High specific surface area (~2600 $m^2\ g^{-1}$), efficient free carrier mobility (~10 000 $cm^2\ V^{-1}\ s^{-1}$ even at low temperature), excellent thermal conductivity (~3000 to 5000 $W\ m^{-1}\ k^{-1}$) and notably high optical transmittance with very low reflectance increase the visible light-harvesting properties and enhance the promise for the fabrication of several energy-conversion devices.[83–85] To be very specific, 2D-graphene nanosheets have efficient active catalytic sites on the interface, which can be combined with traditional photocatalysts for efficient charge separation and photochemical redox reactions. Beyond traditional graphene, its most exciting derivatives, *i.e.*, graphene oxide (GO), reduced graphene oxide (r-GO) and their functional hybrids, possess several advantages over pristine graphene. Low-cost synthesis techniques, promising chemistry due to efficient

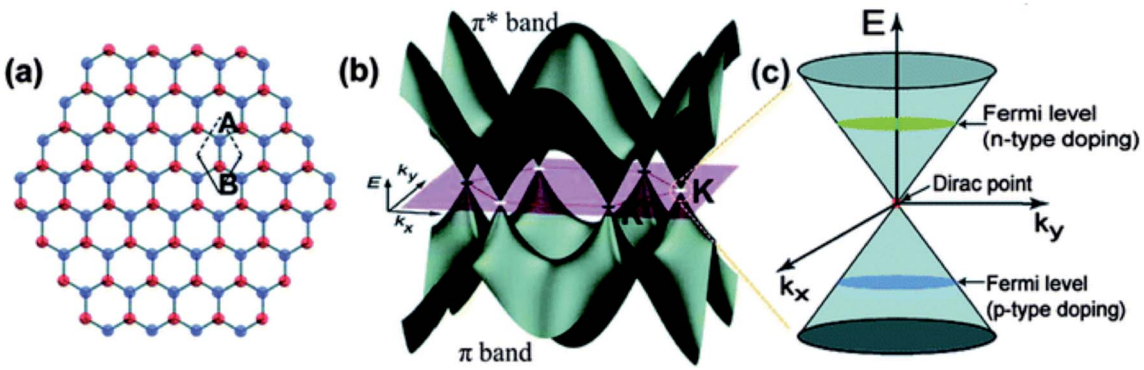

Fig. 9 (a) Hexagonal lattice of graphene with two carbon atoms (A, B) per unit cell; (b) π and π* electronic bands in graphene; (c) linear dispersion of the band structure and Dirac point of graphene. Reprinted with permission from ref. 81. Copyright 2010, American Chemical Society.

surface functional groups and modified semiconducting properties make graphene-based materials advantageous over traditional photocatalytic materials.[27,86]

Depending on the structure–property correlation, two-dimensional graphene-based materials can act as electron acceptors, electron mediators, or directly as catalysts for photocatalytic solar water splitting. The two-dimensional monolayer structure of graphene is sp^2-hybridized and it is formed by combining S, P_x and P_y orbitals on each carbon atom that is covalently bonded (σ-bonding) with three surrounding carbon atoms. The remaining $2P_z$ orbital of each carbon atom, perpendicular to the 2D-graphene plane forms delocalized π and π* orbitals (Fig. 9b). These are called valence band and conduction band orbitals, respectively. Two-dimensional monolayer graphene is considered as a semimetal and/or zero bandgap energy semiconductor, because of the overlap between the valence band and conduction band at the Dirac points (Fig. 9c);[81,87–89] as a result, the conductivity of graphene is extremely high.[90] However, the state of the Fermi level at Dirac points can be tuned by controlling the doping (*i.e.* p-type and n-type doping) inside the 2-D graphene plane.[91] Specifically, in the case of p-type doping the Fermi level is below the Brillouin zone, while for n-type doping, it is above the Brillouin zone. Therefore, through specific doping, the electronic features of graphene can be critically controlled.[92,93] In particular, the zero-band gap feature of graphene is due to the symmetrical nature of the two carbon atoms in one unit cell. As a result, pristine graphene is not suitable to act as an efficient photocatalyst.[79] Therefore, it is crucial to open the band gap of graphene by breaking the lateral, in-plane lattice symmetry in terms of morphological and/or chemical modifications. For example, the replacement of some carbon atoms from the hexagonal plane of the graphene monolayer by some heteroatoms (*e.g.* N, S, P, *etc.*) can break the crystal symmetry and open up band gap between π and π* orbitals. Symmetry can also be broken by transforming the defect-free monolayer of graphene into 3-D aggregates, 2-D graphene nanoribbons and, most commonly, GO.[79,81] Although pure GO is an insulator, the wide bandgap can be tuned by the controlled reduction of GO to the two-dimensional sheet-like reduced GO.[86,94] In this regard, Mathkar *et al.* investigated the controlled reduction of GO to a wide range of reduced GO by using hydrazine vapor.[95] It is noteworthy that the bandgap can be tuned from 3.5 eV to 1.0 eV by this typical method. Along the same lines, Mattevi *et al.* investigated the gradual evolution of the sp^2 domain into the GO nanosheet by varying the extent of thermal reduction.[96] Finally, they achieved a mechanistic model where they proposed that 100% transformation towards the sp^2 domain is not possible (Fig. 10a–d); there will be always some extent of sp^3 hybridized amorphous domain or defects. Ratiometric proportions of sp^2 and sp^3 domains control the overall photophysics, *i.e.*, light absorption, exciton generation, charge separation, and free carrier diffusion towards the active sites for photochemical redox reactions. Furthermore, the enhanced oxygenated functionality between the sp^2-hybridized island of the 2D graphene plane can create a forbidden electronic band of 2.7 eV due to the

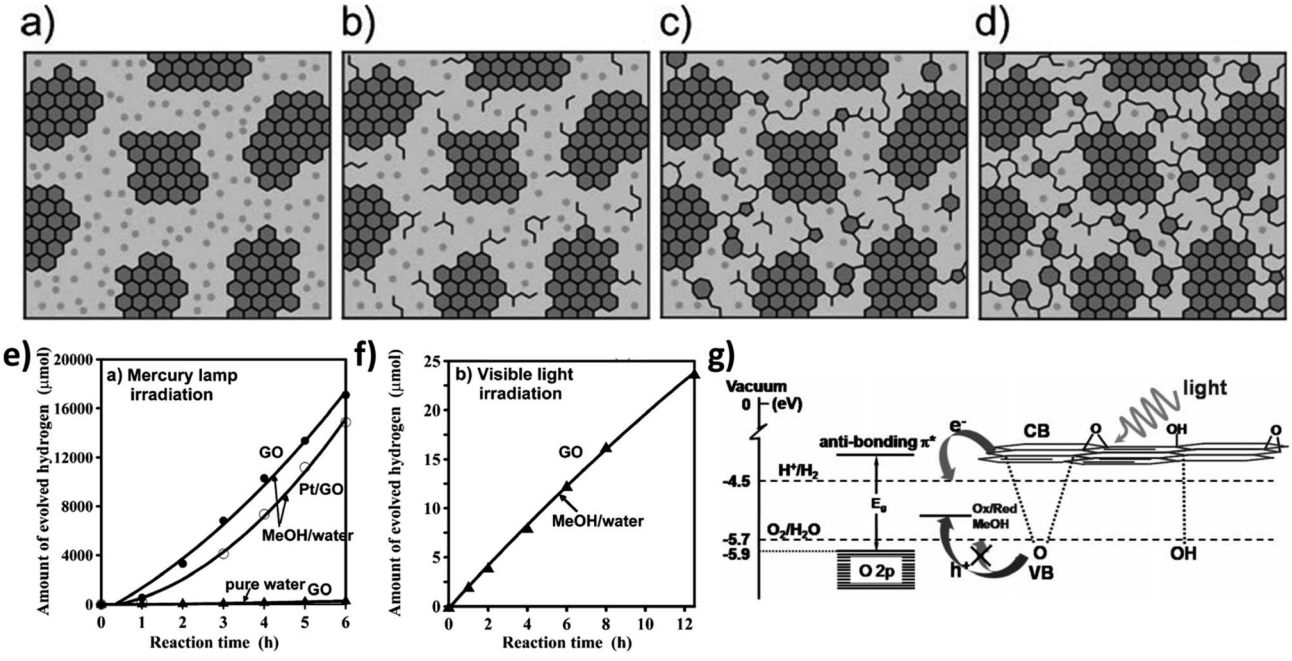

Fig. 10 Schematic representation of the formation of GO at different stages of thermal reduction: (a) room temperature; (b) ~100 °C; (c) ~220 °C; (d) ~500 °C [dark gray: sp^2 domain; light gray: sp^3 domain]. Reprinted with permission from ref. 96. Copyright 2009, WILEY-VCH Verlag GmbH & Co. KGaA, Weinheim. (e) Time course of H_2 evolution from aqueous methanol solution and pure water by photocatalyst under mercury-lamp irradiation. (f) H_2 evolution from aqueous methanol solution by GO with visible light irradiation. (g) Schematic representation of hydrogen production from graphene oxide in the presence of MeOH. Reprinted with permission from ref. 97. Copyright 2010, WILEY-VCH Verlag GmbH & Co. KGaA, Weinheim.

molecular orbital interactions between carbon atoms and oxygen-containing functional groups. However, crystallographic defects throughout the graphene domain can eventually decrease the overall conductivity. Therefore, a trade-off between the defect-related enhancement of photocatalytic active sites and free carrier transport throughout the defined aromatic domain is crucial for the optimization of graphene-based materials.

Considering the semiconducting nature, photoinduced electrons can be promoted to the conduction band of bare r-GO and can be further utilized for redox reactions.[27] Yeh *et al.* investigated the role of r-GO for photocatalytic hydrogen evolution reaction under UV-Vis light (400 Watt high-pressure mercury lamp) from 20% methanol–water mixture;[97] the hydrogen production rate is completely negligible from pure water (Fig. 10e). With 6 h of light irradiation, pristine r-GO can produce 17 000 μmol of hydrogen, while it is comparatively low (280 μmol) in the presence of 5 wt% Pt loading. This anomalous behavior is due to the reduction of active surface groups by 'Pt' nanoparticles. Photoinduced electrons not only reduce protons, but can also reduce the oxygenated surface functional groups, which can reduce the bandgap during the light irradiation. However, the visible light activity (>420 nm) is comparatively less due to inefficient visible light absorption (Fig. 10f). The calculated apparent quantum efficiency for hydrogen production decreases from 2.7% to 0.01% under visible light irradiation. The bandgap energy of GO depends on the number of oxygenated sites in the GO network. The conduction band edge, which is mainly formed by the anti-bonding π* orbital, has higher energy than that needed for proton reduction, thus leading to electron injection into the solution phase for H_2 generation. However, the valence band edge of GO (mainly O 2p orbital) may not be positive enough to oxidize water to O_2 and is neutralized by the sacrificial reagent methanol (Fig. 10g).

Beyond the above mentioned approaches, one of the most common approaches to tune the potential of the valence band maxima and conduction band minima is the doping of heteroatoms (*e.g.* N, B, P, S, *etc.*) inside the sp^2 hybridized domain of 2D-GO. Therefore, even within the localized aromatic domain, one can introduce n-type and/or p-type conductivities by incorporating different heteroatoms as dopants. Consequently, the two-dimensional GO network can act as a platform for both oxidative and reductive half-reactions. As a result, one can develop suitable conditions for overall photocatalytic solar water splitting. Therefore, single-doping with one particular hetero atom and co-doping with multiple hetero atoms can open up several avenues for light-induced reactions.[98]

Garcia and co-workers prepared P-doped graphene by the pyrolysis of $H_2PO_4^-$-modified alginate at 900 °C under an inert atmosphere and demonstrated the visible-light-induced hydrogen production reaction.[99] Alginate is a naturally abundant polysaccharide that is commonly available in the cell walls of brown algae. An aqueous suspension of alginate can form a gel in the presence of various amounts of $H_2PO_4^-$ at neutral pH (Fig. 11a). The alginate gel was pyrolized for graphitization and was further mechanically exfoliated under sonication to get well-defined P-doped two-dimensional graphene. Incorporation of 'P' inside the carbon-containing aromatic domain can enhance the visible light absorption. Detailed XPS studies and ^{31}P NMR analysis suggested that the incorporation of 'P' in the

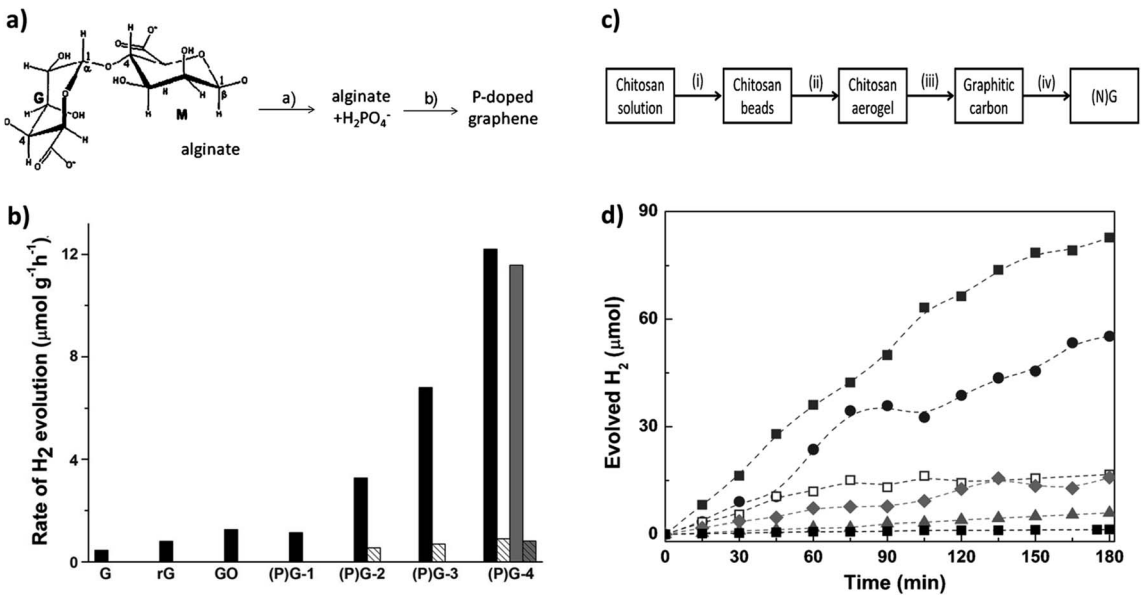

Fig. 11 (a) Schematic representation of the preparation of P-doped graphene. (b) Rate of hydrogen evolution for samples of graphene, reduced G, GO, (P)G-1, (P)G-2, (P)G-3, (P)G-4, and (P)G-4 (third use) from an aqueous methanol solution (30 v/v%). Reprinted with permission from ref. 99. Copyright 2013, WILEY-VCH Verlag GmbH & Co. KGaA, Weinheim. (c) Synthesis of nitrogen-doped graphene [N(G)] mentioning different steps. (d) Hydrogen evolution upon 355 nm irradiation in the presence of (N)G obtained from chitosan pyrolysis at different temperatures (■: GO; ▲: NG-200, ◆: NG-400, □: NG-600, ●: NG-800; ■: NG-900). Reprinted with permission from ref. 100. Copyright 2014, WILEY-VCH Verlag GmbH & Co. KGaA, Weinheim.

graphene domain follows a two-step process. The first step is the reduction of PO_4^{3-} to elemental phosphorous, and the second step is the incorporation of elemental 'P' inside the graphene domain. Finally, it was observed that P-doped graphene showed hydrogen production efficiency that was almost one order of magnitude higher as compared to the pure graphene. It is noteworthy that the incorporation of 'P' introduces the semiconducting nature, as well as increases the visible light absorption, which further enhances the photocatalytic hydrogen generation upon irradiation by both UV-Vis and Vis light sources. In the presence of visible light, the hydrogen production efficiency is considerably less; however, it shows potential for acting as a visible light active photocatalyst without using traditional metal-based systems (Fig. 11b).

The incorporation of 'N' as a heteroatom dopant in graphene has been discussed because of the better atomic size compatibility of 'N' with 'C' and the comparatively easier fabrication techniques directly from small precursors by means of a simple bottom-up approach or several deposition techniques. 'N' atoms can be incorporated inside the graphitic domain mainly in three different motifs: (a) graphitic nitrogen covalently bonded with three carbon atoms, (b) pyridinic nitrogen as the edge nitrogen in a six-membered aromatic ring, and (c) pyrrolic nitrogen as the edge nitrogen in a five-membered aromatic ring. Relative proportions of different nitrogen modes inside the graphitic domain critically controlled the overall optoelectronic properties and opened up the scope for optimization as efficient photocatalytic materials.[98] As an example, Lavorato *et al.* has synthesized nitrogen-doped graphene from chitosan using a high-temperature pyrolysis technique.[100] Chitosan has a sugar-like structure that is naturally obtained from the outer shell of several sea animals, and is a single-molecule precursor containing both 'N' and 'C'; therefore, the direct incorporation of 'N' inside the aromatic domain of graphene is quite obvious. Considering this, the relative proportions of 'N' atoms were varied from 16.2% to 5.4% by varying the synthesis temperature from 200 °C to 900 °C respectively. The synthesis steps are highlighted in Fig. 11c. It was observed that varying the amount of 'N' (upon varying the synthesis temperature) has a direct effect on the production of hydrogen. It is noteworthy that at higher pyrolysis temperatures and lower nitrogen content, the samples showed greater hydrogen production efficiencies with both UV and visible light irradiation. This is because at higher temperatures, defect-free aromatic domains can be created, while at lower temperatures the graphene domains consist of more defect states with several nitrogen functionalities (Fig. 11d). The incorporation of defect states increases the competitive recombination sites. Furthermore, the simultaneous co-doping by different heteroatoms can also increase visible-light-induced photocatalytic hydrogen generation efficiencies due to their efficient solar light-harvesting properties and free carrier transport properties.[101] In addition, it can eventually enhance the active sites for photochemical half-cell reactions.

The major challenge of using graphene/graphene oxide solely as a photocatalyst is the lack of visible light absorption. To address this issue, one can utilize visible light-absorbing dye molecules as an efficient photosensitizer for GO-based materials.[27] Dye sensitization has become one of the most popular and robust approaches for harvesting visible light from the solar spectrum. Common oxygenated surface functional groups/edge groups of GO introduce negative surface charges. Therefore, visible-light-absorbing positively charged dye molecules can be easily attached to the negatively charged GO system by means of electrostatic forces of attraction. In this regard, Latorre-Sanchez *et al.* fabricated a metal-free hybrid system by combining GO with positively charged $[Ru(bpy)_3]^{2+}$ dye molecules.[102] The dye molecules were intercalated inside the layered structure of GO. The GO functionality was critically controlled by the extent of the oxidation process. In general, this fluorophore molecule has a strong visible-light absorption cross section. Therefore, under excitation at 532 nm, intercalated dye molecules can get excited, followed by photoinduced electron transfer processes to GO. This can be further utilized through the reductive half reaction for hydrogen generation. However, the visible-light active photocatalytic efficiency can be further increased by using GO as a scaffold for 'Pt' by using eosin Y as the visible-light sensitizer.[103] It is noteworthy that the calculated quantum yield of hydrogen evolution can achieve up to 9.3% by using 520 nm light. Graphene oxide can also indirectly enhance the hydrogen production as an efficient electron acceptor and electron mediator while combined with a traditional metal-based photocatalyst; a detailed discussion is beyond the scope of this review.

5. One-dimensional carbon nanotubes and their hybrids

As efficient one-dimensional carbon-based nanomaterials for photocatalytic applications, both single-walled and multi-walled carbon nanotubes have been investigated in detail over the past few decades.[104] This is because of their interesting morphological features, large surface area and efficient free carrier mobility.[105] The most common approaches to utilize both single-walled and multi-walled carbon nanotubes (SWCNT or MWCNT) are as follows: (a) making hybrids with metal-based inorganic semiconductors,[106] (b) dye-sensitized CNT for photocatalytic hydrogen generation;[107] (c) making all carbon-based hybrids with other carbon-based semiconductors.[108]

To date, several attempts have been made to make hybrids by combining metal oxides with both SWCNT and MWCNT for photocatalytic hydrogen generation.[109] In these typical hybrids, upon light irradiation, inorganic semiconductors transfer photoinduced electrons to the CNT, followed by efficient free-electron migration towards the interfacial redox-active sites for hydrogen generation. As a metal-free approach, visible-light absorbing ionic dye molecules can also be electrostatically attached to a chemically-treated 1D CNT system. Normally, both the single-walled and multi-walled carbon nanotubes are insoluble in solvent medium. Physical and chemical treatment can increase the defects and/or chemical functionalities on the surface of the CNT. Acid-based controlled oxidation is one of the most common methods for increasing the oxygenated

functional groups on the surface of CNT. In this regard, Lu and co-workers investigated the photocatalytic hydrogen generation of the MWCNT@Pt composite by using eosin Y as a photosensitizer. The surface functionalization of MWCNT has been critically controlled by using varied concentrations of HNO_3. Selective oxidation of MWCNT by dilute HNO_3 helps the charge separation process after the photosensitization of the electrostatically attached eosin Y dye molecules; it was further confirmed by photoluminescence quenching of eosin Y molecules. Photoinduced electrons quickly transfer from eosin Y to MWCNT, which eventually inhibits the recombination process of e^-/h^+ pairs; as a result, the photocatalytic hydrogen generation efficiency increases.[107]

Both SWCNT and MWCNT can be combined with the g-C_3N_4 system for hydrogen evolution. In a previous report, Ge *et al.* reported a specific composite by the thermal treatment of a cyanamide and MWCNT mixture. Bare g-C_3N_4 shows a characteristic absorption band corresponding to 2.7 eV, while visible light absorption gradually increases upon combining g-C_3N_4 with MWCNT. The extent of visible light absorption increases with the increase in the MWCNT content. Notably, this typical composite system shows visible light-induced hydrogen generation even without using any metal co-catalyst. In addition, it shows excellent stability upon long-term light irradiation.[104] In a similar way, Fornasiero and coworkers investigated the photocatalytic hydrogen generation efficiency of a heptazine-based g-C_3N_4–CNT composite by varying the wall number of CNT, *i.e.*, single-walled, double-walled and multi-walled CNTs (SWCNT, DWCNT and MWCNT, respectively). SWCNT show higher hydrogen generation efficiency as compare to the double- or multi-walled system under solar and specific visible light irradiation. This is due to the efficient charge separation from CN to SWCNT, as the charge separation efficiency is inversely proportional to the wall number of CNTs.[108]

In general, beyond traditional carbon nanotubes, other 1D carbon-based materials (for example carbon nanofibers, g-C_3N_4 nanofibers, *etc.*) can act as an efficient (photo) catalyst or (photo) co-catalyst while combined with traditional 0D, 1D and 2D semiconductors.[110] However, the major components of all these composite systems are metal-based semiconducting materials; metal-free approaches were also investigated very recently.[111] Qu and coworkers recently developed mesoporous g-C_3N_4 nanofibers, followed by the incorporation of nitrogen-rich carbon content through the post-polymerization of pyrrole molecules (Fig. 12a).[112] Detailed elemental analysis from XPS studies showed that the overall structure remained almost similar to g-C_3N_4. C and N were homogeneously distributed throughout the overall nanofiber. However, the relative carbon content with respect to nitrogen increased from 0.72 to 0.86 after carbon incorporation through polypyrrole. Furthermore,

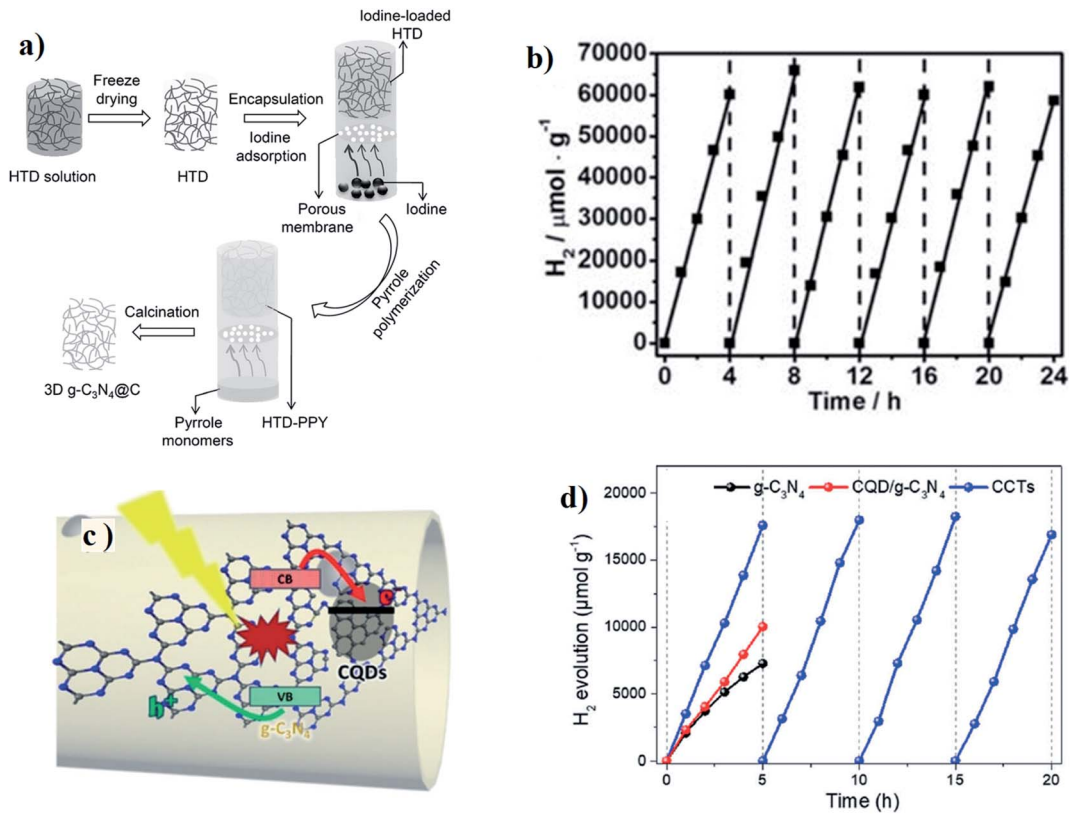

Fig. 12 (a) Experimental procedure for the fabrication of 3D g-C_3N_4@C; (b) stable hydrogen evolution by g-C_3N_4@C without co-catalyst ($\lambda > 420$ nm). Reprinted with permission from ref. 112. Copyright 2016, WILEY-VCH Verlag GmbH & Co. KGaA, Weinheim. (c) Schematic representation of the photocarrier separation in CCTs. (d) Time course of H_2 evolution experiments for g-C_3N_4 and CCTs under visible light irradiation ($\lambda > 420$ nm). Reprinted with permission from ref. 113. Copyright 2018, WILEY-VCH Verlag GmbH & Co. KGaA, Weinheim.

carbon incorporation inside the g-C_3N_4 fibers enhanced the overall absorption spectra and the calculated bandgap decreased from ~2.7 eV to ~2.2 eV. Photoluminescence quenching and enhanced photocurrent generation further supported the charge separation, followed by the electron transfer process towards the surface, which reduced the charge recombination process and enhanced the hydrogen generation. This typical composite system showed almost 4 times enhanced hydrogen production (16 885 μmol g^{-1} h^{-1}) as compared to the pristine system, while the redox cycle was completed by using TEOA as a hole scavenger (Fig. 12b). The hydrogen production quantum yield reached almost ~14% under 420 nm excitation wavelength. To date, this is one of the most efficient of all carbon-based composite systems that can produce this much hydrogen through a metal-free approach.

Wang *et al.*[113] recently fabricated carbon quantum dots (CQDs) implanted in the surface plane of g-C_3N_4 nanotubes by the thermal polymerization of freeze-dried urea and CQDs precursor (Fig. 12c). The CQD-implanted g-C_3N_4 nanotubes (CCTs) could simultaneously facilitate the photoelectron transport and suppresses charge recombination through their specially coupled heterogeneous interface. The electronic structure and morphology were optimized in the CCTs, contributing to greater visible light absorption and a weakened barrier to the photocarrier transfer. As a result, the CCTs exhibited efficient photocatalytic performance under light irradiation with a high H_2 production rate of 3538.3 mmol g^{-1} h^{-1} and a notable quantum yield of 10.94% at 420 nm (Fig. 12d).

6. Zero-dimensional carbon dots/graphene QDs for photocatalytic water splitting

To date, several advancements have been made on various traditional carbon-based materials (*e.g.*, g-C_3N_4 and their hybrid materials, graphene-based materials, CNT, carbon nanofibers, *etc.*) as efficient metal-free catalysts for specific solar light-induced water splitting; however, there are also several disadvantages. Notably, the common limiting factors include a high probability of charge recombination in the interfacial region, low solubility in water due to larger polymeric structure, lack of visible light absorption, the necessity of very specific sacrificial agents to complete the redox cycle, and hard synthetic procedures including high-temperature condensation from very limited molecular precursors.[32,33]

Considering the above limitations, zero-dimensional (0-D) luminescent carbon dots and/or graphene quantum dots (CDs or GQDs) can be an emerging class of alternative materials for photocatalytic hydrogen generation.[32,34,114–116] However, this is still in the nascent stage and several challenges have to be addressed for their optimization. Fluorescent carbon dots and/or graphene quantum dots have become interesting candidates in biologically relevant imaging and sensing devices due to their highly luminescent behaviors, complete benign nature, high solubility in aqueous medium, efficient photostability, *etc.*[117–121] However, significant efforts have been made very recently in optoelectronic, catalytic and energy storage devices.[34]

Unlike other carbon-based nanomaterials (*e.g.*, g-C_3N_4, graphene, carbon nanotubes, carbon nanofibers, *etc.*), CDs have been considered as a large class of 0-D carbon-based nanomaterials, with several other heteroatom functionalities. Depending on the synthesis parameters, the intriguing features of CDs can be drastically varied. In general, all the synthesis procedures can mainly be categorized into two different pathways, *i.e.*, top-down and bottom-up synthesis approaches (Fig. 13).[101,122] In the top-down approaches, the zero-dimensional carbon dots/graphene QDs are prepared by breaking down various highly defined carbon materials through different physical or chemical treatments. Typically, physical exfoliations or chemical oxidations from sp^2 hybridized ordered carbon-based materials (*e.g.*, graphene, graphene oxide, CNT, *etc.*) can maintain highly defined graphitic domains inside the zero-dimensional dot-like structure.[97] Most of the time, it consists of a few-layered graphene-like structure with larger lateral dimensions.[123] The ordered aromatic domain helps the overall charge transfer process, which is again crucial for overall photocatalysis. However, CDs/graphene QDs synthesized from top-down approach have less surface functional groups, which make them hard to solubilize in water; therefore, additional surface functionalization is required to increase the aqueous solubility.[124] On the other hand, bottom-up-based approaches consist of the thermal pyrolysis of small molecules by heat treatment (mainly hydrothermal/microwave treatment). It is a stepwise carbonization process, by which we can form carbogenic dots by the stepwise removal of H_2O and CO_2.[125–128] The typical CDs/graphene QDs synthesized from the common bottom-up approach generally possess both sp^2 and sp^3 domains inside the tiny dots (<10 nm), which critically regulates both the radiative exciton recombination and charge separation processes.[129,130] Intrinsic oxygen and nitrogen-containing functionalities at the exterior surface enhance their solubility in polar media and also facilitates the accumulation of free charges on the surface.[115,131] However, undefined morphologies, defect states due to the greater extent of the amorphous domain and the formation of specific molecular fluorophores enhance the competitive recombination processes that eventually decrease the number of the free carriers for photocatalysis. Therefore, the overall optimization of the typical CDs/graphene QDs in terms of the detailed structure–property correlation is crucial for their future applications.

Teng and his group, for the first time, demonstrated the role of N-doped graphene QDs acting as a direct photocatalyst for overall water splitting under visible light.[114] N-doping has been done by treating GO with NH_3 at higher temperatures, followed by the transformation of GO to graphene QDs by chemical oxidation methods. As a result, the N-doped graphene sheet-like structure was achieved, while the crystal surface contained oxygen-containing functional groups. N-doping increased the visible light absorption and n-type conductivity throughout the sp^2 hybridized aromatic domain, whereas the oxygenated surface functionality introduced p-type conductivity into the basal plane of GO QD, resulting in the photochemical diode-like

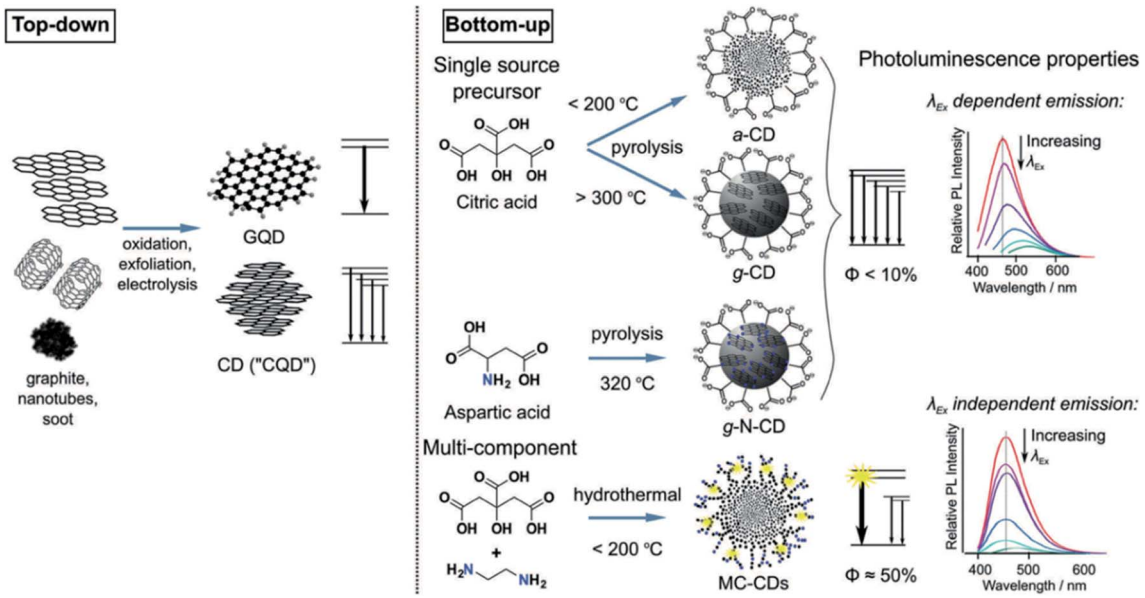

Fig. 13 Schematic representation of top-down and bottom-up approaches to graphene QDs and/or CDs and their corresponding PL spectra. Reprinted with permission from ref. 122. Copyright 2017, The Royal Society of Chemistry.

structure. The oxygen functionality could act as an electron reservoir suitable for the reductive half-reaction, *i.e.*, proton reduction to the hydrogen molecule. Simultaneously, the free hole residing on the nitrogen atom inside the aromatic domain promotes the oxidative half-reaction, *i.e.*, the production of oxygen from water (Fig. 14a). The sp^2 hybridized carbon cluster acts as a molecular junction between the p-type and n-type domains. Finally, overall photocatalytic water splitting towards H_2 and O_2 can be achieved (Fig. 14b). This carbon-containing molecular junction can also act as the recombination site for electron–hole pairs, resulting in the high photoluminescence intensity of N-doped graphene oxide QDs.

In a very recent report, Yan *et al.*[132] demonstrated two different methods to systematically tune the bandgap of GQDs; these are as follows: (a) enlarging the sp^2 hybridized conjugated domain by interacting with additional polyaromatic molecules; (b) introducing a nonbonding orbital between the π and π^* orbitals of GQDs upon attaching electron-donating functional groups. This is based on the formation of the 'Z-scheme' structure by connecting n-type and p-type domains through the sp^2 hybridized carbon network as depicted before.[114] Lowering

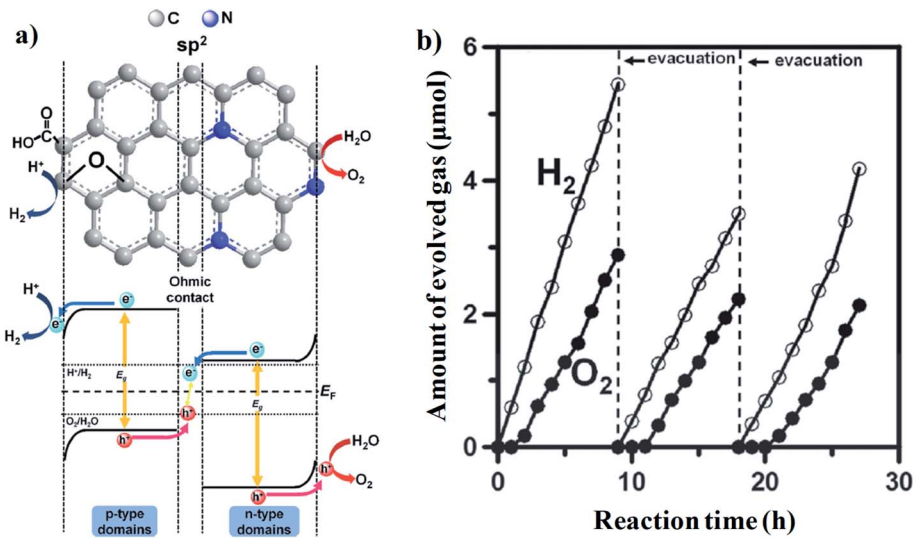

Fig. 14 (a) Schematic representation of the intrinsic hybrid heterostructure inside N-doped graphene QDs. (b) Visible light (420 nm < λ < 800 nm)-induced production of hydrogen and oxygen over NGO-QDs from pure water. Reprinted with permission from ref. 114. Copyright 2014, WILEY-VCH Verlag GmbH & Co. KGaA, Weinheim.

the bandgap enhances the visible light absorption, while introducing the 'Z scheme' structure increases the charge separation. Therefore, by both these modifications, one will be able to increase the overall photocatalysis. Chemical etching through strong acid has been utilized to fabricate graphene-QDs with a lot of oxygenated surface functionalities. The extended π-conjugated domain was achieved by treating graphene oxide QDs with four different polyaromatic compounds, namely, *o*-phenylenediamine (OPD), 2,3-diaminonaphthalene (DNPT23), 1,8-diaminonaphthalene (DNPT18) and 1,1′-bi(2-naphthalene) (BNPTL), through typical solvothermal methods.[132] A gradual bathochromic shift was observed for the absorption band around the 550 nm to 600 nm region, with the following descending order: GO-QDs < GO-OPD < GO-DNPT23 < GO-DNPT 18 < GO-BNPTL. This absorption shoulder specifically corresponds to the n–π* transition from the pyrazine-N of the external polyaromatic ring towards the π* orbital of GOQDs and it gradually shifted towards the longer wavelength region with the increasing size of the polyaromatic molecules attached to the main conjugated domain of GOQDs. On the other hand, the bandgap can be alternatively narrowed down by introducing electron-donating groups like *p*-anisidine (Anln-OCH_3), 4-(trifluoromethoxy)aniline (Anln-OCF_3) and 4-(trichloromethoxy) aniline (Anln-$OCCl_3$). A similar red shifting of the absorption shoulder peak supports the narrowing of the bandgap due to the incorporation of electron-donating groups (N, F and Cl). The

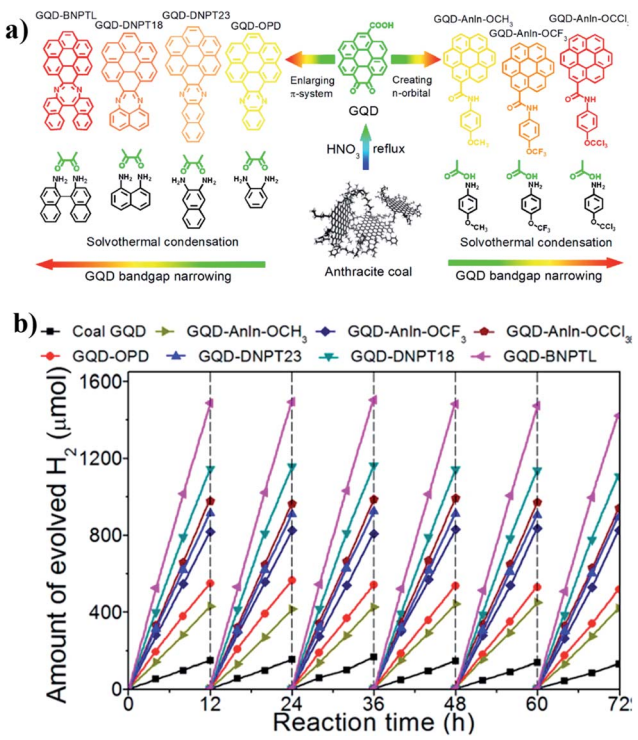

Fig. 15 (a) A schematic representation of the bandgap tuning of GQDs by increasing the π-conjugated domain upon combining with polyaromatic rings, or by introducing an intermediate n-orbital *via* conjugation with electron-donating groups. (b) Hydrogen evolution rates of different GQDs under visible light. Reprinted with permission from ref. 132. Copyright 2014, American Chemical Society.

intrinsic Z-scheme structure and standard redox potentials for water splitting and CO_2 reduction are aligned within the range of the CBM and VBM of the GQDs; therefore, all these GOQDs can be utilized for both these photocatalytic reactions. A detailed schematic representation and hydrogen production rates are depicted in Fig. 15.[132]

Beyond these highly defined graphene QDs/CDs obtained *via* top-down synthesis, the CDs obtained from the bottom-up approach can also be utilized for photocatalytic water splitting, either as a catalyst or as a sensitizer to harvest solar light, followed by the photosensitization of another catalyst for water splitting. CDs specifically synthesized by the bottom-up approach have similarities to both semiconducting QDs and molecular fluorophores.[123,133] One can balance these two types of characteristic features of CDs by simply tuning the synthesis parameters and precursor concentration; as such, the CDs can be directly optimized as a photocatalysts for water splitting. However, most of the previous reports discussed the specific applications of CDs upon combining with metal-based photosensitizers.[134] Very few recent reports have highlighted the applicability of pure CDs as photocatalysts, even without using a metal-based co-catalyst.[135,136] The major challenges are to increase the visible-light absorption and critically control the charge separation process over competitive recombination processes. These challenges can be overcome by modifying the heteroatom functionalities both inside the core aromatic domain and also as surface functional groups. In a recent report, Xu *et al.* demonstrated the excitation-independent down and up-conversion behaviors of conjugated CQDs synthesized by the typical hydrothermal-based bottom-up approach from citric acid and urea.[135] A detailed understanding of absorption, photoluminescence and excitation spectra could explain the different transition channels for different photoinduced electrons, followed by their recombination with photogenerated holes in the same energy level. The three transition channels are very well distinguished: (a) near band–edge transition, (b) transition from amino groups on the surface, and (c) multi-photon transition from surface defect states (Fig. 16a). Multiple transition channels of photoinduced electrons act as long-term electron reservoirs by reducing the quick recombination process, which indirectly helps the hole scavenging process *in situ* by surface functional groups, resulting in efficient photocatalytic hydrogen generation. Chen *et al.* observed very high photocatalytic hydrogen production (hydrogen production quantum yield 21%) from ammonia-treated N-GQDs.[115] This is due to the lone electron pair of the nitrogen atom coming from the surface-attached amino and/or amide group, which can enhance the effective conjugated domain and also prolong the lifetime of photogenerated electrons due to the transition from the singlet to the triplet state close to the conduction band minima. Therefore, in the presence of hole scavengers, long-living electrons in the excited state can promote the reductive half-reaction for hydrogen generation (Fig. 16b).

The critical design of the N atom functionality and its inclusion mode inside the aromatic domain for carbon-based materials (CDs/GQDs, *etc.*) can increase their potential for application as a new class of alternative metal-free catalysts. In

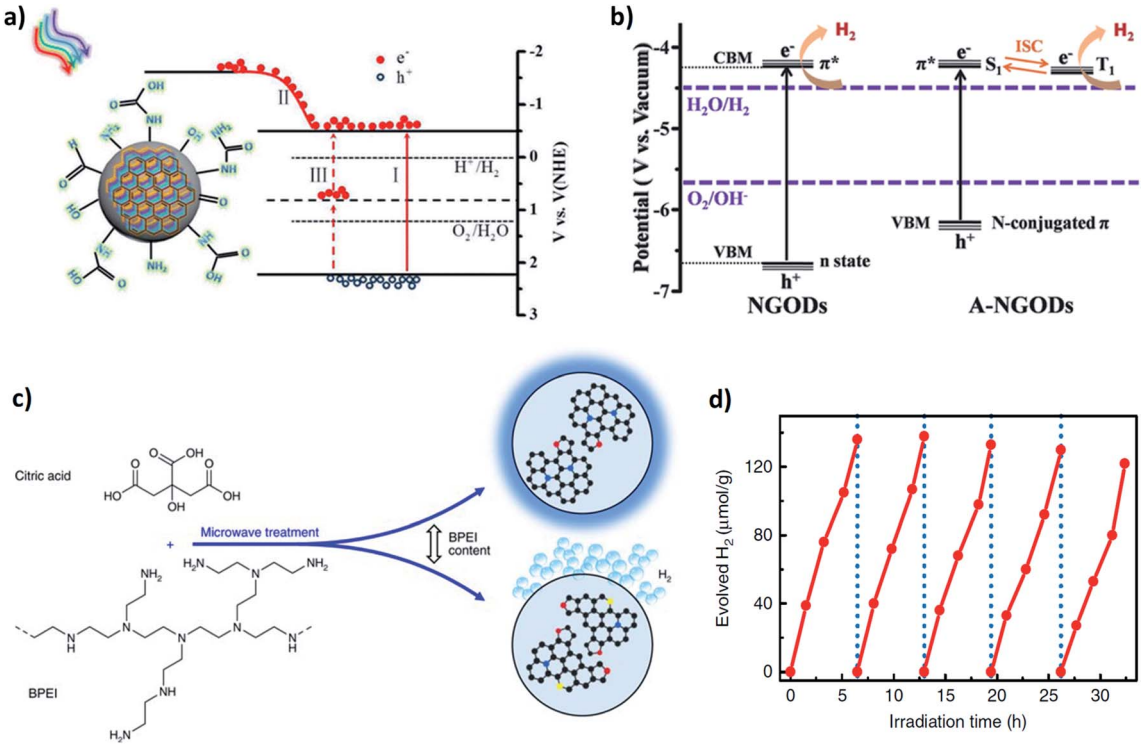

Fig. 16 (a) Qualitative band structure diagram and schematic representation of three types of electron transition modes: (i) near band edge transition, (ii) electron donation from functional amine groups, (iii) multiphoton active up-conversion. Reprinted with permission from ref. 135. Copyright 2016, American Chemical Society. (b) Energy level diagrams of NGODs and A-NGODs relative to the levels for proton reduction and water oxidation potential. Reprinted with permission from ref. 115. Copyright 2016, WILEY-VCH Verlag GmbH & Co. KGaA, Weinheim. (c) Schematic representation of the microwave-assisted synthesis procedure of N-doped CDs upon varying the concentration of the BPEI precursor (polycyclic aromatic molecules inside the CDs with different nitrogen atom positioning, *i.e.*, graphitic nitrogen (blue), pyrrolic nitrogen (red), and pyridinic nitrogen (yellow), respectively); (d) photocatalytic H_2 generation by CDs under Xe lamp irradiation in 5-cycles. Reprinted with permission from ref. 136. Copyright 2017, The Authors.

a recent report, Bhattacharyya and his coworkers explained the critical role of aromatic nitrogen atom on the trade-off between photoluminescence and photocatalytic hydrogen generation by simply varying the precursor concentration in a simple microwave-assisted bottom-up approach (Fig. 16c).[136] The amount of N-precursor concentration (branched polyethyleneimine; BPEI) determines the degree of nitrogen incorporation and the different inclusion modes within the CDs. At an intermediate level of BPEI, a relative proportion of aromatic domain with a greater extent of graphitic nitrogen enhances the relative photoluminescence QY, while at an extremely high concentration of BPEI, the nitrogen atoms are located primarily at the edge sites of the aromatic domains (mainly as pyrrolic nitrogen). Pyrrolic nitrogen introduces specific edge defects that attract photogenerated electrons, resulting in efficient charge separation and enhanced photocatalytic hydrogen generation from water (Fig. 16d).

CDs/GQDs can also act as efficient light-harvesting moieties to photosensitize surface-attached catalysts for efficient photocatalytic processes.[122] However, the use of CDs as an efficient visible light-sensitive photosensitizer is practically very difficult, as one has to form a composite device for this particular purpose.[123,137] Reisner and his group made an inexpensive composite of CDs with a 3d transition metal-based molecular proton reduction catalyst for photocatalytic hydrogen production (Fig. 17a).[32,122] For example, a composite system of amorphous CDs with molecular nickel catalyst ($[Ni(P_2N_2)_2]^{2+}$) can achieve H_2 production activity up to 398 μmol g_{CQD}^{-1} h^{-1} under full solar light irradiation at one Sun intensity.[32] In this typical composite, CQD can efficiently harvest solar light in the UV and visible regions, followed by efficient electron transfer towards the molecular Ni catalyst. Furthermore, visible light absorption can be effectively tuned by controlling the relativistic proportions of the nitrogen-doped aromatic domain with respect to the amorphous domain.[138] Nitrogen sites in the aromatic domain can also enhance the hole scavenging process, which increases the lifetime of the photogenerated free electrons. These free electrons were further accumulated for the proton reduction reaction. Transient absorption data showed a prominent transient absorption signal near 550 nm and 650 nm (characteristic transient absorption signals of CDs) with a picosecond time-scale for more than 90% of the excited state (Fig. 17b).[138] However, the rest of the electrons in their excited states possessed a long time-span (up to the microsecond to second time-scale), which supports the formation of long-lived photogenerated electrons. The gradual enhancement of the graphitic domain further enhanced the hole scavenging

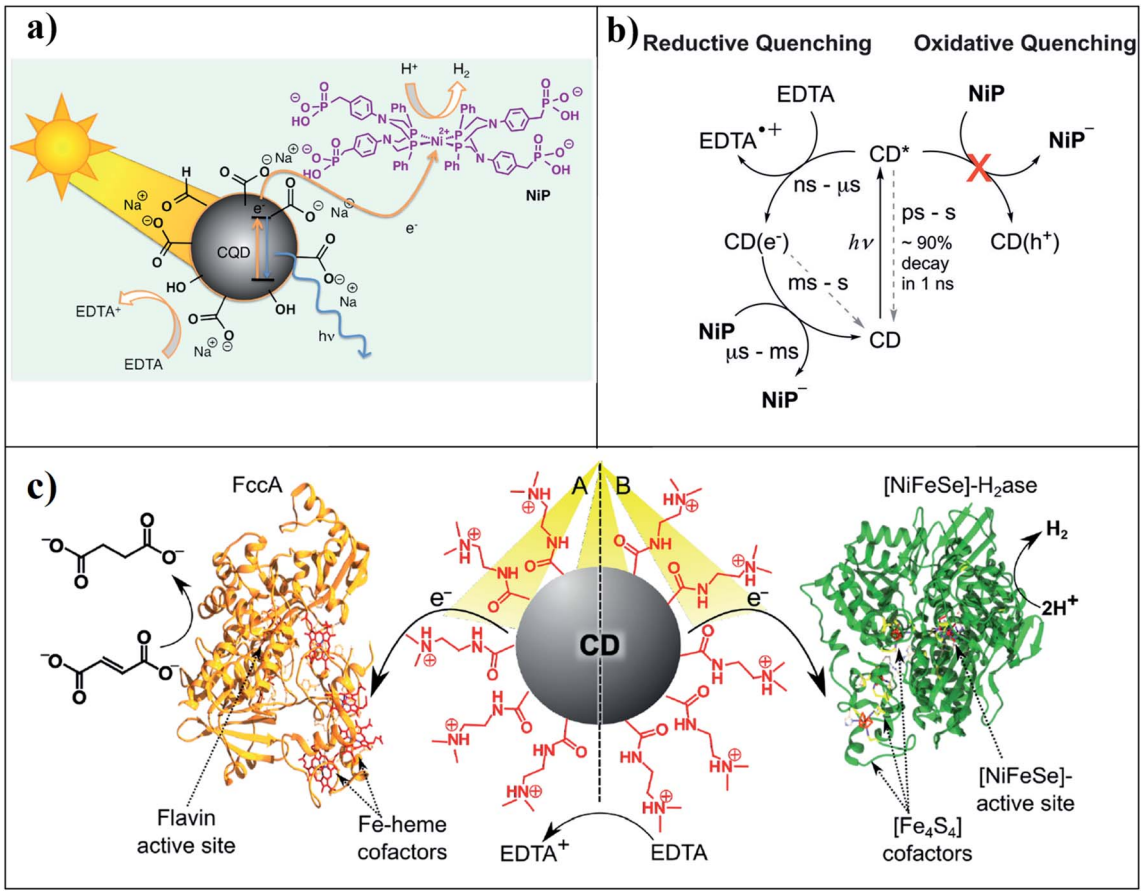

Fig. 17 (a) Representation of solar H_2 production using the hybrid CQD–NiP system. Reprinted with permission from ref. 32. Copyright 2017, American Chemical Society. (b) Time-scales of charge transfer processes in CD/NiP photosystems. Productive charge transfer steps are indicated with solid black arrows, and recombination reactions with gray dashed arrows. Reprinted with permission from ref. 138. Copyright 2017, WILEY-VCH Verlag GmbH & Co. KGaA, Weinheim. (c) Representations of the photocatalytic systems of the positively charged CD–$NHMe^{2+}$ with a fumarate reductase (FccA; system A) or a [NiFeSe]-hydrogenase (H_2ase; system B) and their catalytic activity. Reprinted with permission from ref. 139. Copyright 2016, American Chemical Society.

process, resulting in efficient hydrogen generation up to an IQE of ~5%.

A semi-biological photocatalytic system can be developed by combining CDs (acting as a synthetic light-harvesting unit) with an isolated redox active enzyme or biological organism for enzymatic catalysis; more specifically, for catalytic hydrogen generation. However, optimizing the surface functionality is crucial for the electron transfer from the abiotic synthetic moiety towards biological counterparts. In a recent report,[139] positively charged CDs with tertiary amine groups on the surface were electrostatically attached to the redox-active enzymes, a fumarate reductase (FccA; Fig. 17c, system A), or [NiFeSe]-hydrogenase [H_2ase; Fig. 17c, system B]. Upon irradiation, positively charged CDs transfer electrons toward the negatively charged FccA or H_2ase for the reduction of fumarate to succinate and protons to H_2, respectively. Redox-active enzymes possess surface-exposed co-factors that act as an entry point for electrons from positively charged CDs upon light irradiation. The electrons then shuttled towards the active site for hydrogen generation. However, photoinduced electron transfer from CDs to redox-active biological moieties is quite challenging because of the several surface functional groups on the surface of CDs, which can increase the competitive non-radiative recombination process. Therefore, a proper optimization process is desirable for these specific composites.

7. Summary and outlook

Searching for new materials for photocatalytic solar water splitting has become the current emerging field of material research. Improvement of the materials especially depends on the main aspects of visible-light absorption, charge separation and interfacial photochemical reactions. Several advancements have already been made with traditional metal oxides and other inorganic semiconductors. In the presence of metal co-catalysts and sufficient hole scavengers for the completion of the redox cycle, the external quantum efficiency for hydrogen evolution can be achieved, almost close to 100%, by using traditional metal-based catalysts.[140] However, basic challenges regarding heavy metal-based toxicity, environmental sustainability and the costly approach of using expensive noble metals make their

practical applicability questionable. Therefore, it is essential to find alternative materials that can overcome all the challenges, and can subsequently be applied in hydrogen production and for overall water splitting without the further use of any metal-based counterpart. Considering this, we have critically discussed the carbon-based nanomaterials and their hybrids as alternative metal-free photocatalysts for solar-light-driven H_2 generation, followed by the most challenging part, the simultaneous production of H_2 and O_2 through full water splitting. The current discussion specifically includes the recent developments of the following systems: (a) carbon nitrides and their hybrids, (b) 2D graphene-based materials, (c) 1D carbon nanotubes and/or carbon nanofibers and their hybrids, (d) 0D graphene QDs/carbon dots.

It has already been established that g-C_3N_4 has become the most promising carbon-based material for solar hydrogen generation. Notably, stand-alone carbon nitride has already achieved almost ~30% hydrogen production efficiency upon intrinsic modification/optimization. However, recent developments based on the carbon nitride heterostructure have shown almost 80% hydrogen production efficiency. It is encouraging that the future development of this particular aspect will further quantitatively increase the performance. However, in most of the cases, the oxidative half reaction is satisfied by applying specific hole scavenger/electron-donating molecules. The applicability of g-C_3N_4 for full water splitting without using a metal catalyst still has not been investigated properly. Therefore, future research should be carried out in this specific direction, where one should focus on the tailored design of g-C_3N_4 for complete charge separation and their accumulation on the surface for full water splitting.

Other sp^2 hybridized carbon-based materials (*e.g.* graphene, graphene oxide, carbon nanotubes *etc.*) cannot solely act as an efficient photocatalyst for solar water splitting. These types of materials are specifically used as co-catalysts or charge-transporting materials. However, all carbon-based (metal-free) heterojunction hybrids, especially those focusing on Z-scheme technology, already have potential as a new class of photocatalysts. The dye-sensitized approach can be another alternative approach in this regard.

Heteroatom-doped zero-dimensional CDs/graphene QDs are among the most promising candidates for photocatalytic hydrogen evolution, as well as complete water splitting, without using any further metal-based co-catalyst. However, the photocatalytic efficiency is very low compared to the traditional metal-based photocatalyst; future research is necessary for this particular aspect. Lack of visible light absorption and competitive recombination processes make it inefficient. Therefore, to utilize CDs/graphene QDs solely as a photocatalyst, it is crucial to optimize these materials for more visible light absorption, greater extent of charge separation and their survival while competing with the recombination processes, and finally diffusion towards the surface for photocatalysis. However, a detailed structure–property correlation has not been well investigated to date for CDs/graphene QDs. It is challenging because the structural features of CDs are very complicated since this is the combination of both the

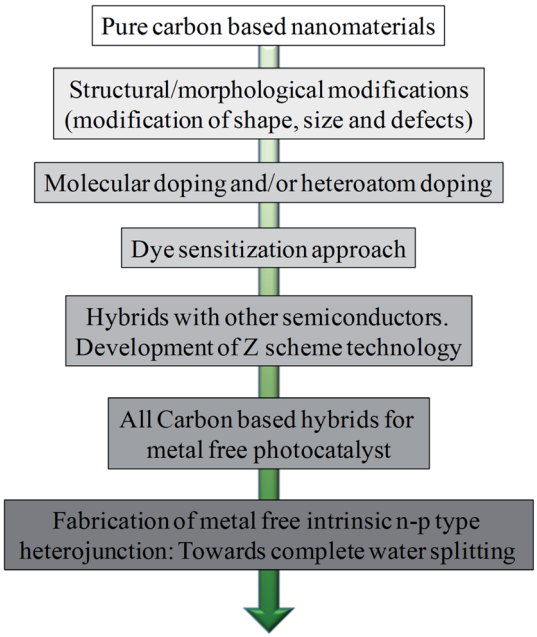

Fig. 18 Scheme of the recent progress and challenges in solar water splitting by carbon-based nanomaterials.

smaller fluorophore molecules and the larger extended aromatic domains; the complex interplay between these two domains critically controls the overall excitonic features and charge separation kinetics. Therefore, it is crucial to focus on the structural and elemental features, as well as the intrinsic bonding motifs, followed by understanding the fate of free carriers by means of highly resolved time domain/frequency domain absorption and fluorescence study by laser spectroscopy. Considering the recent advancement, the formation of all carbon-based heterojunctions by combining CQDs with other carbon-based nanomaterials has already shown greater hydrogen production efficiency as compared to the single system. The intrinsic n–p-type dyad-like structure can also be developed by incorporating different heteroatoms inside CQDs, which will eventually enhance the visible light absorption as well as charge separation process (Fig. 18). Further research is needed in this direction. A theoretical understanding is also essential for the structural optimization of this typical material. For example, detailed density functional theory (DFT) calculations will help us to unravel the atomic level surface chemistry, which will be beneficial for the further optimization of these materials. Furthermore, the theoretical investigation of heteroatom bonding motifs inside the carbon-containing aromatic domain and their critical role in energy level alignments will help us to investigate intrinsic photophysical behaviors, followed by crucial structure–property correlations. Photocatalytic water splitting may not be suitable for the current global energy demand but the continuous development on improved efficiency, environmental sustainability and cost-effectiveness will certainly increase the potential as one of the most efficient approaches to renewable energy resources.

Conflicts of interest

There are no conflicts of interest to declare.

Acknowledgements

Authors would like to acknowledge DST-SERB for financial support (grant number-SRG/2019/000026). S. B. would like to acknowledge IISER Berhampur for initiation grant (IG/21082018/B0035). K. B. would like to acknowledge IISER Berhampur for offering postdoctoral fellowship.

References

1 F. Perera, *Int. J. Environ. Res. Public Health*, 2018, **15**, 16.
2 https://netl.doe.gov/coal/crosscutting/energy-storage.
3 M. Ball and M. Wietschel, *The Hydrogen Economy: Opportunities and Challenges*, Cambridge University Press, Cambridge, 2009.
4 S. Dahl and I. Chorkendorff, *Nat. Mater.*, 2012, **11**, 100–101.
5 N. S. Lewis and D. G. Nocera, *Proc. Natl. Acad. Sci. U. S. A.*, 2006, **103**, 15729–15735.
6 P. V. Kamat and J. Bisquert, *J. Phys. Chem. C*, 2013, **117**, 14873–14875.
7 P. V. Kamat and J. A. Christians, *J. Phys. Chem. Lett.*, 2015, **6**, 1917–1918.
8 M. G. Walter, E. L. Warren, J. R. McKone, S. W. Boettcher, Q. Mi, E. A. Santori and N. S. Lewis, *Chem. Rev.*, 2010, **110**, 6446–6473.
9 A. Vasileff, Y. Zheng and S. Z. Qiao, *Adv. Energy Mater.*, 2017, **7**, 1700759.
10 M. Faizal, L. Chuah, C. Lee, A. Hameed, J. Lee and M. Shankar, *Journal of Mechanical Engineering Research and Developments*, 2019, **42**, 35–46.
11 H. Ahmad, S. K. Kamarudin, L. J. Minggu and M. Kassim, *Renewable Sustainable Energy Rev.*, 2015, **43**, 599–610.
12 M. Grätzel, *Nature*, 2001, **414**, 338–344.
13 M. Z. Rahman, C. W. Kwong, K. Davey and S. Z. Qiao, *Energy Environ. Sci.*, 2016, **9**, 709–728.
14 M. Rahman, K. Davey and S.-Z. Qiao, *Adv. Funct. Mater.*, 2017, **27**, 1606129.
15 J. K. Stolarczyk, S. Bhattacharyya, L. Polavarapu and J. Feldmann, *ACS Catal.*, 2018, **8**, 3602–3635.
16 A. Fujishima and K. Honda, *Nature*, 1972, **238**, 37–38.
17 R. Daghrir, P. Drogui and D. Robert, *Ind. Eng. Chem. Res.*, 2013, **52**, 3581–3599.
18 X. Chen, S. Shen, L. Guo and S. S. Mao, *Chem. Rev.*, 2010, **110**, 6503–6570.
19 Z. Bian, T. Tachikawa, P. Zhang, M. Fujitsuka and T. Majima, *J. Am. Chem. Soc.*, 2014, **136**, 458–465.
20 S. Kundu and V. Polshettiwar, *ChemPhotoChem*, 2018, **2**, 796–800.
21 T. Simon, N. Bouchonville, M. J. Berr, A. Vaneski, A. Adrović, D. Volbers, R. Wyrwich, M. Döblinger, A. S. Susha, A. L. Rogach, F. Jäckel, J. K. Stolarczyk and J. Feldmann, *Nat. Mater.*, 2014, **13**, 1013–1018.
22 P.-Y. Kuang, P.-X. Zheng, Z.-Q. Liu, J.-L. Lei, H. Wu, N. Li and T.-Y. Ma, *Small*, 2016, **12**, 6735–6744.
23 X. Li, J. Yu and M. Jaroniec, *Chem. Soc. Rev.*, 2016, **45**, 2603–2636.
24 S. Y. Tee, K. Y. Win, W. S. Teo, L.-D. Koh, S. Liu, C. P. Teng and M.-Y. Han, *Adv. Sci.*, 2017, **4**, 1600337.
25 S. Kundu and A. Patra, *Chem. Rev.*, 2017, **117**, 712–757.
26 N. L. Reddy, V. N. Rao, M. Vijayakumar, R. Santhosh, S. Anandan, M. Karthik, M. V. Shankar, K. R. Reddy, N. P. Shetti, M. N. Nadagouda and T. M. Aminabhavi, *Int. J. Hydrogen Energy*, 2019, **44**, 10453–10472.
27 Y. Yao, *Visible-Light Photocatalysis of Carbon-Based Materials*, IntechOpen Limited, London, 2018.
28 B. Adeli and F. Taghipour, *Appl. Catal., A*, 2016, **521**, 250–258.
29 T. Jafari, E. Moharreri, A. Amin, R. Miao, W. Song and S. Suib, *Molecules*, 2016, **21**, 900.
30 N. Serpone, A. V. Emeline, V. K. Ryabchuk, V. N. Kuznetsov, Y. M. Artem'ev and S. Horikoshi, *ACS Energy Lett.*, 2016, **1**, 931–948.
31 H. Zhao, L. Jin, Y. Zhou, A. Bandar, Z. Fan, A. O. Govorov, Z. Mi, S. Sun, F. Rosei and A. Vomiero, *Nanotechnology*, 2016, **27**, 495405.
32 B. C. M. Martindale, G. A. M. Hutton, C. A. Caputo and E. Reisner, *J. Am. Chem. Soc.*, 2015, **137**, 6018–6025.
33 Z. Zhang, T. Zheng, X. Li, J. Xu and H. Zeng, *Part. Part. Syst. Charact.*, 2016, **33**, 457–472.
34 X. Li, M. Rui, J. Song, Z. Shen and H. Zeng, *Adv. Funct. Mater.*, 2015, **25**, 4929–4947.
35 W.-J. Ong, L.-L. Tan, Y. H. Ng, S.-T. Yong and S.-P. Chai, *Chem. Rev.*, 2016, **116**, 7159–7329.
36 R. A. Marcus, *J. Chem. Phys.*, 1956, **24**, 966–978.
37 H. Kato, K. Asakura and A. Kudo, *J. Am. Chem. Soc.*, 2003, **125**, 3082–3089.
38 S. Yan, L. Wan, Z. Li and Z. Zou, *Chem. Commun.*, 2011, **47**, 5632–5634.
39 H. Kisch, *Semiconductor photocatalysis: principles and applications*, John Wiley & Sons, 2015.
40 A. Kubacka, M. Fernández-García and G. Colón, *Chem. Rev.*, 2012, **112**, 1555–1614.
41 A. Thomas, A. Fischer, F. Goettmann, M. Antonietti, J.-O. Müller, R. Schlögl and J. M. Carlsson, *J. Mater. Chem.*, 2008, **18**, 4893–4908.
42 X. Wang, K. Maeda, A. Thomas, K. Takanabe, G. Xin, J. M. Carlsson, K. Domen and M. Antonietti, *Nat. Mater.*, 2009, **8**, 76–80.
43 B. V. Lotsch, M. Döblinger, J. Sehnert, L. Seyfarth, J. Senker, O. Oeckler and W. Schnick, *Chem.–Eur. J.*, 2007, **13**, 4969–4980.
44 D. J. Martin, K. Qiu, S. A. Shevlin, A. D. Handoko, X. Chen, Z. Guo and J. Tang, *Angew. Chem., Int. Ed.*, 2014, **53**, 9240–9245.
45 W. Ho, Z. Zhang, W. Lin, S. Huang, X. Zhang, X. Wang and Y. Huang, *ACS Appl. Mater. Interfaces*, 2015, **7**, 5497–5505.
46 J. Zhang, G. Zhang, X. Chen, S. Lin, L. Möhlmann, G. Dołęga, G. Lipner, M. Antonietti, S. Blechert and X. Wang, *Angew. Chem., Int. Ed.*, 2012, **51**, 3183–3187.

47 A. Mishra, A. Mehta, S. Basu, N. P. Shetti, K. R. Reddy and T. M. Aminabhavi, *Carbon*, 2019, **149**, 693–721.
48 J. Zhang, M. Zhang, S. Lin, X. Fu and X. Wang, *J. Catal.*, 2014, **310**, 24–30.
49 S. Chu, Y. Wang, Y. Guo, J. Feng, C. Wang, W. Luo, X. Fan and Z. Zou, *ACS Catal.*, 2013, **3**, 912–919.
50 Y.-N. Liu, C.-C. Shen, N. Jiang, Z.-W. Zhao, X. Zhou, S.-J. Zhao and A.-W. Xu, *ACS Catal.*, 2017, **7**, 8228–8234.
51 M. Zhang, Y. Duan, H. Jia, F. Wang, L. Wang, Z. Su and C. Wang, *Catal. Sci. Technol.*, 2017, **7**, 452–458.
52 X. Li, G. Hartley, A. J. Ward, P. A. Young, A. F. Masters and T. Maschmeyer, *J. Phys. Chem. C*, 2015, **119**, 14938–14946.
53 Y. Liu, C. Xiao, Z. Li and Y. Xie, *Adv. Energy Mater.*, 2016, **6**, 1600436.
54 H. Yu, R. Shi, Y. Zhao, T. Bian, Y. Zhao, C. Zhou, G. I. N. Waterhouse, L.-Z. Wu, C.-H. Tung and T. Zhang, *Adv. Mater.*, 2017, **29**, 1605148.
55 H. Wang, X. Zhang, J. Xie, J. Zhang, P. Ma, B. Pan and Y. Xie, *Nanoscale*, 2015, **7**, 5152–5156.
56 Q. Tay, P. Kanhere, C. F. Ng, S. Chen, S. Chakraborty, A. C. H. Huan, T. C. Sum, R. Ahuja and Z. Chen, *Chem. Mater.*, 2015, **27**, 4930–4933.
57 W. Wu, J. Zhang, W. Fan, Z. Li, L. Wang, X. Li, Y. Wang, R. Wang, J. Zheng, M. Wu and H. Zeng, *ACS Catal.*, 2016, **6**, 3365–3371.
58 V. W.-h. Lau, I. Moudrakovski, T. Botari, S. Weinberger, M. B. Mesch, V. Duppel, J. Senker, V. Blum and B. V. Lotsch, *Nat. Commun.*, 2016, **7**, 12165.
59 V. W.-h. Lau, V. W.-z. Yu, F. Ehrat, T. Botari, I. Moudrakovski, T. Simon, V. Duppel, E. Medina, J. K. Stolarczyk, J. Feldmann, V. Blum and B. V. Lotsch, *Adv. Energy Mater.*, 2017, **7**, 1602251.
60 Q. Han, B. Wang, Y. Zhao, C. Hu and L. Qu, *Angew. Chem., Int. Ed.*, 2015, **54**, 11433–11437.
61 Z. Tong, D. Yang, Z. Li, Y. Nan, F. Ding, Y. Shen and Z. Jiang, *ACS Nano*, 2017, **11**, 1103–1112.
62 Q. Gu, Y. Liao, L. Yin, J. Long, X. Wang and C. Xue, *Appl. Catal., B*, 2015, **165**, 503–510.
63 B. Long, Y. Zheng, L. Lin, K. A. Alamry, A. M. Asiri and X. Wang, *J. Mater. Chem. A*, 2017, **5**, 16179–16188.
64 G. Zhang, M. Zhang, X. Ye, X. Qiu, S. Lin and X. Wang, *Adv. Mater.*, 2014, **26**, 805–809.
65 Z.-F. Huang, J. Song, L. Pan, Z. Wang, X. Zhang, J.-J. Zou, W. Mi, X. Zhang and L. Wang, *Nano Energy*, 2015, **12**, 646–656.
66 Y.-P. Zhu, T.-Z. Ren and Z.-Y. Yuan, *ACS Appl. Mater. Interfaces*, 2015, **7**, 16850–16856.
67 S. Guo, Z. Deng, M. Li, B. Jiang, C. Tian, Q. Pan and H. Fu, *Angew. Chem., Int. Ed.*, 2016, **55**, 1830–1834.
68 J. Ran, T. Y. Ma, G. Gao, X.-W. Du and S. Z. Qiao, *Energy Environ. Sci.*, 2015, **8**, 3708–3717.
69 Z. Luo, M. Zhou and X. Wang, *Appl. Catal., B*, 2018, **238**, 664–671.
70 L. Zhang, Y. Zhang, R. Shi, S. Bao, J. Wang, A. Amini, B. N. Chandrashekar and C. Cheng, *Materials Today Energy*, 2017, **5**, 91–98.
71 K. Dai, L. Lu, Q. Liu, G. Zhu, X. Wei, J. Bai, L. Xuan and H. Wang, *Dalton Trans.*, 2014, **43**, 6295–6299.
72 Z. Tong, D. Yang, J. Shi, Y. Nan, Y. Sun and Z. Jiang, *ACS Appl. Mater. Interfaces*, 2015, **7**, 25693–25701.
73 X. Zhang, B. Peng, S. Zhang and T. Peng, *ACS Sustainable Chem. Eng.*, 2015, **3**, 1501–1509.
74 Y. Chen, J. Li, Z. Hong, B. Shen, B. Lin and B. Gao, *Phys. Chem. Chem. Phys.*, 2014, **16**, 8106–8113.
75 W. Zhou, T. Jia, H. Shi, D. Yu, W. Hong and X. Chen, *J. Mater. Chem. A*, 2019, **7**, 303–311.
76 J. Liu, Y. Liu, N. Liu, Y. Han, X. Zhang, H. Huang, Y. Lifshitz, S.-T. Lee, J. Zhong and Z. Kang, *Science*, 2015, **347**, 970–974.
77 W. Che, W. Cheng, T. Yao, F. Tang, W. Liu, H. Su, Y. Huang, Q. Liu, J. Liu, F. Hu, Z. Pan, Z. Sun and S. Wei, *J. Am. Chem. Soc.*, 2017, **139**, 3021–3026.
78 M. Zhu, S. Kim, L. Mao, M. Fujitsuka, J. Zhang, X. Wang and T. Majima, *J. Am. Chem. Soc.*, 2017, **139**, 13234–13242.
79 G. Lu, K. Yu, Z. Wen and J. Chen, *Nanoscale*, 2013, **5**, 1353–1368.
80 K. S. Novoselov, A. K. Geim, S. V. Morozov, D. Jiang, M. I. Katsnelson, I. V. Grigorieva, S. V. Dubonos and A. A. Firsov, *Nature*, 2005, **438**, 197–200.
81 P. Avouris, *Nano Lett.*, 2010, **10**, 4285–4294.
82 M. Inagaki, Y. A. Kim and M. Endo, *J. Mater. Chem.*, 2011, **21**, 3280–3294.
83 X. Huang, X. Qi, F. Boey and H. Zhang, *Chem. Soc. Rev.*, 2012, **41**, 666–686.
84 Q. Xiang, J. Yu and M. Jaroniec, *Chem. Soc. Rev.*, 2012, **41**, 782–796.
85 K. P. Loh, Q. Bao, P. K. Ang and J. Yang, *J. Mater. Chem.*, 2010, **20**, 2277–2289.
86 K. P. Loh, Q. Bao, G. Eda and M. Chhowalla, *Nat. Chem.*, 2010, **2**, 1015–1024.
87 A. H. Castro Neto, F. Guinea, N. M. R. Peres, K. S. Novoselov and A. K. Geim, *Rev. Mod. Phys.*, 2009, **81**, 109–162.
88 R. Garg, N. K. Dutta and N. R. Choudhury, *Nanomaterials*, 2014, **4**, 267–300.
89 T. Ohta, A. Bostwick, T. Seyller, K. Horn and E. Rotenberg, *Science*, 2006, **313**, 951.
90 X. Zhang, B. R. S. Rajaraman, H. Liu and S. Ramakrishna, *RSC Adv.*, 2014, **4**, 28987–29011.
91 X.-K. Kong, C.-L. Chen and Q.-W. Chen, *Chem. Soc. Rev.*, 2014, **43**, 2841–2857.
92 G. Wu, X. Tang, M. Meyyappan and K. W. C. Lai, *Appl. Surf. Sci.*, 2017, **425**, 713–721.
93 T. Schiros, D. Nordlund, L. Pálová, D. Prezzi, L. Zhao, K. S. Kim, U. Wurstbauer, C. Gutiérrez, D. Delongchamp, C. Jaye, D. Fischer, H. Ogasawara, L. G. M. Pettersson, D. R. Reichman, P. Kim, M. S. Hybertsen and A. N. Pasupathy, *Nano Lett.*, 2012, **12**, 4025–4031.
94 S. Vempati and T. Uyar, *Phys. Chem. Chem. Phys.*, 2014, **16**, 21183–21203.
95 A. Mathkar, D. Tozier, P. Cox, P. Ong, C. Galande, K. Balakrishnan, A. Leela Mohana Reddy and P. M. Ajayan, *J. Phys. Chem. Lett.*, 2012, **3**, 986–991.

96 C. Mattevi, G. Eda, S. Agnoli, S. Miller, K. A. Mkhoyan, O. Celik, D. Mastrogiovanni, G. Granozzi, E. Garfunkel and M. Chhowalla, *Adv. Funct. Mater.*, 2009, **19**, 2577–2583.
97 T.-F. Yeh, J.-M. Syu, C. Cheng, T.-H. Chang and H. Teng, *Adv. Funct. Mater.*, 2010, **20**, 2255–2262.
98 D. W. Chang and J.-B. Baek, *Chem.–Asian J.*, 2016, **11**, 1125–1137.
99 M. Latorre-Sánchez, A. Primo and H. García, *Angew. Chem., Int. Ed.*, 2013, **52**, 11813–11816.
100 C. Lavorato, A. Primo, R. Molinari and H. Garcia, *Chem.–Eur. J.*, 2014, **20**, 187–194.
101 P. Tian, L. Tang, K. S. Teng and S. P. Lau, *Mater. Today Chem.*, 2018, **10**, 221–258.
102 M. Latorre-Sánchez, C. Lavorato, M. Puche, V. Fornés, R. Molinari and H. Garcia, *Chem.–Eur. J.*, 2012, **18**, 16774–16783.
103 S. Min and G. Lu, *J. Phys. Chem. C*, 2011, **115**, 13938–13945.
104 L. Ge and C. Han, *Appl. Catal., B*, 2012, **117–118**, 268–274.
105 F. Wang, G. Dukovic, L. E. Brus and T. F. Heinz, *Science*, 2005, **308**, 838.
106 Y. Takaguchi, T. Tajima and H. Miyake, in *Nanocarbons for Energy Conversion: Supramolecular Approaches*, Springer, 2019, pp. 205–218.
107 Q. Li, L. Chen and G. Lu, *J. Phys. Chem. C*, 2007, **111**, 11494–11499.
108 K. C. Christoforidis, Z. Syrgiannis, V. La Parola, T. Montini, C. Petit, E. Stathatos, R. Godin, J. R. Durrant, M. Prato and P. Fornasiero, *Nano Energy*, 2018, **50**, 468–478.
109 K. Dai, X. Zhang, K. Fan, P. Zeng and T. Peng, *J. Nanomater.*, 2014, **2014**, 694073.
110 J. Ge, Y. Zhang and S.-J. Park, *Materials*, 2019, **12**, 1916.
111 X. Liu and L. Dai, *Nat. Rev. Mater.*, 2016, **1**, 16064.
112 Q. Han, B. Wang, J. Gao and L. Qu, *Angew. Chem., Int. Ed.*, 2016, **55**, 10849–10853.
113 Y. Wang, X. Liu, J. Liu, B. Han, X. Hu, F. Yang, Z. Xu, Y. Li, S. Jia, Z. Li and Y. Zhao, *Angew. Chem., Int. Ed.*, 2018, **57**, 5765–5771.
114 T.-F. Yeh, C.-Y. Teng, S.-J. Chen and H. Teng, *Adv. Mater.*, 2014, **26**, 3297–3303.
115 L.-C. Chen, C.-Y. Teng, C.-Y. Lin, H.-Y. Chang, S.-J. Chen and H. Teng, *Adv. Energy Mater.*, 2016, **6**, 1600719.
116 P. Yang, J. Zhao, J. Wang, H. Cui, L. Li and Z. Zhu, *RSC Adv.*, 2015, **5**, 21332–21335.
117 L. Cao, X. Wang, M. J. Meziani, F. Lu, H. Wang, P. G. Luo, Y. Lin, B. A. Harruff, L. M. Veca, D. Murray, S.-Y. Xie and Y.-P. Sun, *J. Am. Chem. Soc.*, 2007, **129**, 11318–11319.
118 C. Ding, A. Zhu and Y. Tian, *Acc. Chem. Res.*, 2014, **47**, 20–30.
119 F. Wang, Y.-h. Chen, C.-y. Liu and D.-g. Ma, *Chem. Commun.*, 2011, **47**, 3502–3504.
120 S. N. Baker and G. A. Baker, *Angew. Chem., Int. Ed.*, 2010, **49**, 6726–6744.
121 S. Y. Lim, W. Shen and Z. Gao, *Chem. Soc. Rev.*, 2015, **44**, 362–381.
122 G. A. M. Hutton, B. C. M. Martindale and E. Reisner, *Chem. Soc. Rev.*, 2017, **46**, 6111–6123.
123 H. Yu, R. Shi, Y. Zhao, G. I. N. Waterhouse, L.-Z. Wu, C.-H. Tung and T. Zhang, *Adv. Mater.*, 2016, **28**, 9454–9477.
124 Y.-P. Sun, B. Zhou, Y. Lin, W. Wang, K. A. S. Fernando, P. Pathak, M. J. Meziani, B. A. Harruff, X. Wang, H. Wang, P. G. Luo, H. Yang, M. E. Kose, B. Chen, L. M. Veca and S.-Y. Xie, *J. Am. Chem. Soc.*, 2006, **128**, 7756–7757.
125 C. X. Guo, D. Zhao, Q. Zhao, P. Wang and X. Lu, *Chem. Commun.*, 2014, **50**, 7318–7321.
126 B. J. Moon, Y. Oh, D. H. Shin, S. J. Kim, S. H. Lee, T.-W. Kim, M. Park and S. Bae, *Chem. Mater.*, 2016, **28**, 1481–1488.
127 M. K. Barman, B. Jana, S. Bhattacharyya and A. Patra, *J. Phys. Chem. C*, 2014, **118**, 20034–20041.
128 F. Pschunder, M. A. Huergo, J. M. Ramallo-López, B. Kommula, F. G. Requejo and S. Bhattacharyya, *J. Phys. Chem. C*, 2020, **124**, 1121–1128.
129 S. Zhu, Y. Song, X. Zhao, J. Shao, J. Zhang and B. Yang, *Nano Res.*, 2015, **8**, 355–381.
130 M. Fu, F. Ehrat, Y. Wang, K. Z. Milowska, C. Reckmeier, A. L. Rogach, J. K. Stolarczyk, A. S. Urban and J. Feldmann, *Nano Lett.*, 2015, **15**, 6030–6035.
131 X. Li, S. Zhang, S. A. Kulinich, Y. Liu and H. Zeng, *Sci. Rep.*, 2014, **4**, 4976.
132 Y. Yan, J. Chen, N. Li, J. Tian, K. Li, J. Jiang, J. Liu, Q. Tian and P. Chen, *ACS Nano*, 2018, **12**, 3523–3532.
133 K. A. S. Fernando, S. Sahu, Y. Liu, W. K. Lewis, E. A. Guliants, A. Jafariyan, P. Wang, C. E. Bunker and Y.-P. Sun, *ACS Appl. Mater. Interfaces*, 2015, **7**, 8363–8376.
134 L. Cao, S. Sahu, P. Anilkumar, C. E. Bunker, J. Xu, K. A. S. Fernando, P. Wang, E. A. Guliants, K. N. Tackett and Y.-P. Sun, *J. Am. Chem. Soc.*, 2011, **133**, 4754–4757.
135 X. Xu, Z. Bao, G. Zhou, H. Zeng and J. Hu, *ACS Appl. Mater. Interfaces*, 2016, **8**, 14118–14124.
136 S. Bhattacharyya, F. Ehrat, P. Urban, R. Teves, R. Wyrwich, M. Döblinger, J. Feldmann, A. S. Urban and J. K. Stolarczyk, *Nat. Commun.*, 2017, **8**, 1401.
137 Y.-Q. Zhang, D.-K. Ma, Y.-G. Zhang, W. Chen and S.-M. Huang, *Nano Energy*, 2013, **2**, 545–552.
138 B. C. M. Martindale, G. A. M. Hutton, C. A. Caputo, S. Prantl, R. Godin, J. R. Durrant and E. Reisner, *Angew. Chem., Int. Ed.*, 2017, **56**, 6459–6463.
139 G. A. M. Hutton, B. Reuillard, B. C. M. Martindale, C. A. Caputo, C. W. J. Lockwood, J. N. Butt and E. Reisner, *J. Am. Chem. Soc.*, 2016, **138**, 16722–16730.
140 S. Pokrant, *Nature*, 2020, **581**, 386–388.